

## ABSTRACT

2 The brain interprets sensory inputs to guide behavior, but behavior itself disrupts sensory inputs.

3 Perceiving a coherent world while acting in it constitutes active perception. For example,

4 saccadic eye movements displace visual images on the retina and yet the brain perceives visual

5 stability. Because this percept of visual stability has been shown to be influenced by prior

6 expectations, we tested the hypothesis that it is Bayesian. The key prediction was that priors

7 would be used more as sensory uncertainty increases. Humans and rhesus macaques reported

8 whether an image moved during saccades. We manipulated both prior expectations and levels

9 of sensory uncertainty. All psychophysical data were compared with the predictions of Bayesian

10 ideal observer models. We found that humans were Bayesian for continuous judgments. For

11 categorical judgments, however, they were anti-Bayesian: they used their priors *less* with

12 greater uncertainty. We studied this categorical result further in macaques. The animals'

13 judgments were similarly anti-Bayesian for sensory uncertainty caused by external, image

14 noise, but Bayesian for uncertainty due to internal, motor-driven noise. A discriminative learning

15 model explained the anti-Bayesian effects. We conclude that active vision uses both Bayesian

16 and discriminative models depending on task requirements (continuous vs. categorical) and the

17 source of uncertainty (image noise vs. motor-driven noise). In the context of previous knowledge

18 about the saccadic system, our results provide an example of how the comparative analysis of

19 Bayesian vs. non-Bayesian models of perception offers novel insights into underlying neural

20 organization.

## SIGNIFICANCE STATEMENT

23 Primate vision deals with two major sources of uncertainty: suppression from eye movements  
24 and noise in the environment. Fortunately, the brain also has prior knowledge about the body  
25 and the world. Systems that exploit such priors more to compensate for greater uncertainty are

26 considered Bayesian. A major theme in neuroscience is that the brain is Bayesian. We tested  
27 that hypothesis for vision in the context of eye movements using an integrated computational-  
28 psychophysical approach. Bayesian models explained perception during movement-induced  
29 noise, but not environmental noise, for which a simpler, “discriminative” model sufficed. We  
30 conclude that primate vision is Bayesian to compensate for intrinsic, but not extrinsic, sources of  
31 uncertainty, an important distinction for designing and interpreting neural studies of perception.

32

### 33 INTRODUCTION

34 Perception can be split into two theoretical stages. Sensory receptors encode physical stimuli  
35 into neural signals (Barlow, 1961) and provide evidence,  $E$ , for the stimulus,  $S$ , to the rest of the  
36 sensory system. The evidence is then decoded to infer the stimulus from the evidence  
37 (Johnson, 2000; Britten et al., 1996) and guide action. Under a probabilistic framework, the goal  
38 of decoding is to infer the probability of the stimulus given the evidence,  $P(S|E)$  (Murphy, 2013).

39 Models of decoding take two broad forms (Ng and Jordan, 2002). Discriminative models  
40 estimate  $P(S|E)$  directly; they draw boundaries between evidence states and map stimulus  
41 states onto them (Rumelhart et al., 1986; Hinton, 1992). Generative models, in contrast, build  
42 models of the world (von Helmholtz, 1924; Rao and Ballard, 1999; Knill and Richards, 1996).  
43 These include the joint probability of the stimulus and the evidence co-occurring,  $P(E, S)$ .  $P(S|E)$   
44 can be derived from the joint probability using Bayes’ rule. As such, Bayesian models are a  
45 common implementation of generative models. Although discriminative and Bayesian models  
46 can combine for perception (Gardner, 2019; Sohn and Jazayeri, 2021; DiCarlo et al., 2021),  
47 Bayesian models have been particularly influential in explaining how sensorimotor systems use  
48 prior knowledge to optimally resolve uncertainty (e.g., Jacobs, 1999; Ernst and Banks, 2002;  
49 Weiss et al., 2002; Knill and Saunders, 2003; Körding and Wolpert, 2004; Jazayeri and  
50 Shadlen, 2010; Girshick et al., 2011; Fetsch et al., 2012; Darlington et al., 2017).

51           Sensory uncertainty may be introduced at the input stage or arise from one's own  
52 movements. Constructing a stable, predictable percept of the world while moving through it  
53 constitutes *active perception* (Gibson, 1966; Bajcsy, 1988). Active perception is fundamental for  
54 behavior and its dysfunction may contribute to psychiatric disorders (Feinberg and Guazzelli,  
55 1999; Ford and Mathalon, 2005; Thakkar and Rolfs, 2019). An apt model system for studying  
56 active perception is visual processing across saccades in primates (Wurtz et al., 2011; Parr and  
57 Friston, 2017). Each saccade blurs and displaces the visual image on the retinas. To counter  
58 these disruptions, the primate visual system uses a copy of the saccade command, or “corollary  
59 discharge” to suppress the blur and nullify predicted displacements (Wurtz, 2018). At least part  
60 of this process, saccadic suppression of the blur, is the outcome of combining motor and  
61 sensory information across saccades in a Bayes optimal manner (Niemeier et al., 2003;  
62 Crevecoeur and Körding, 2017).

63           Here, we focused on whether Bayesian models are used to correct self-generated retinal  
64 displacements. The primate visual system, using corollary discharge, can predict its inputs after  
65 each saccade (Sommer and Wurtz, 2002; 2006; Vaziri et al., 2006) and compare that prediction  
66 with the postsaccadic visual input (Figure 1a). A match means that a viewed object was stable.  
67 Previous work by Rao et al. (2016) showed that humans use priors about the probability of  
68 object movement for this process. In this study, we asked whether priors are used in a Bayesian  
69 manner, i.e., are they used more with greater sensory uncertainty?

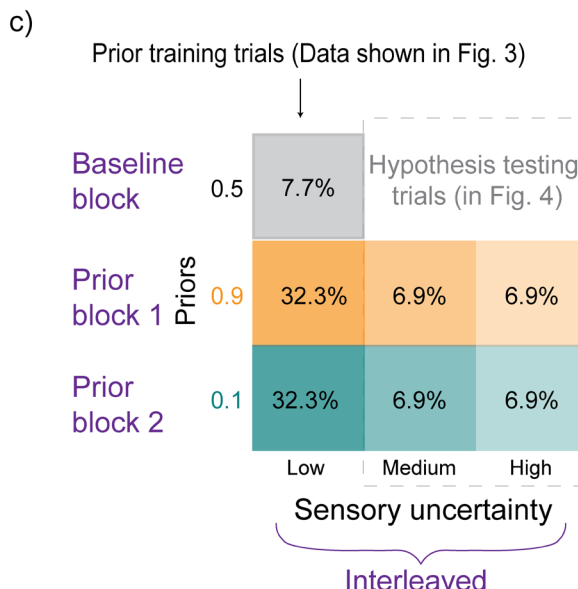
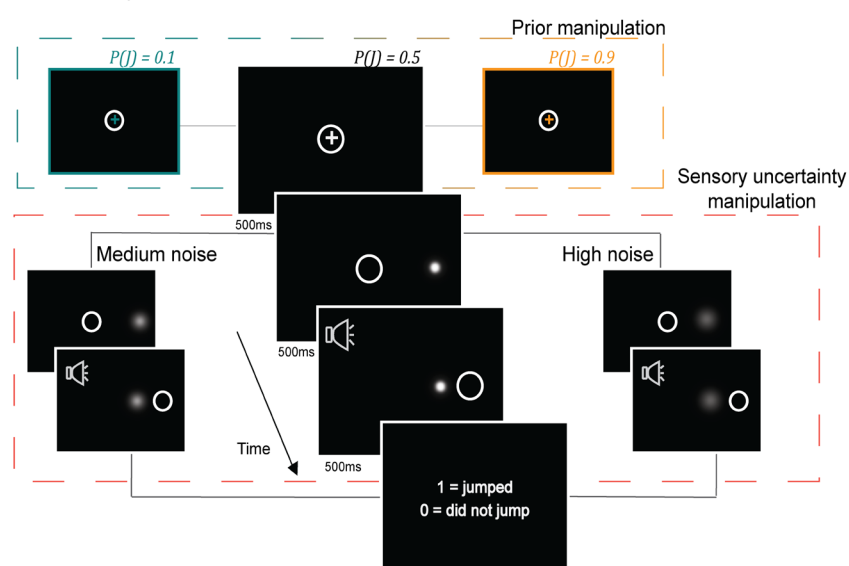
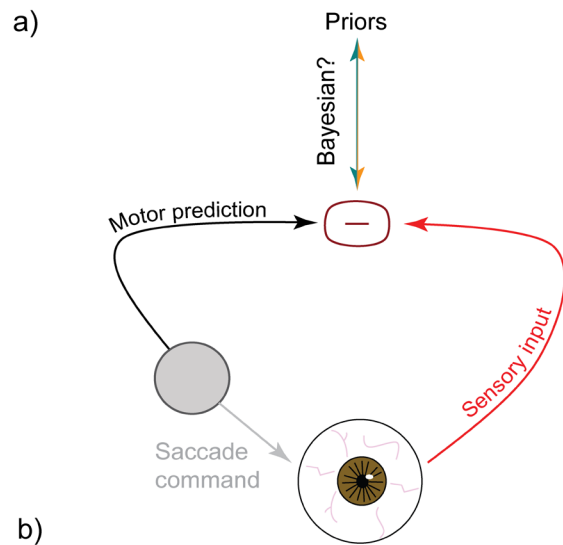


**Figure 1.** Experimental design. a) Judging whether an object is stable or moves during a saccade involves comparing a motor-driven prediction with sensory input. We tested if this process is Bayesian. b) Schematic of the SSD task. Middle, larger panels: “baseline” condition with neutral prior  $P(J) = 0.5$  and low uncertainty (minimal blur). White circle: eye position. High (0.9) and low (0.1) priors were cued by the color of the fixation cross (*top dashed box*). Sensory noise was manipulated by the width of the Gaussian target (*bottom dashed box*). c) Trial breakdown for Experiment 2. Numbers in the boxes indicate the overall proportion of each trial type. Blocks of high and low priors followed a baseline block (black). 70% of trials in the prior blocks (i.e., in the orange or teal rows) were prior-training trials with low uncertainty and priors matched to true jump probability (results shown in Figure 3). For each prior, training trials constituted 32.3% of all trials in the experiment. 30% were hypothesis testing trials with medium and high uncertainty targets. Fixation colors cued the learned priors even though the true jump probability was 0.5 (results shown in Figure 4). Hypothesis testing trials formed 6.9% of all presented trials at each uncertainty level.

First, we evaluated ways to induce sensory uncertainty (*Experiment 1*). Then we extended the paradigm of Rao et al. (2016) to test whether humans are Bayesian when reporting categorically if a stimulus moved or not during a saccade (*Experiment 2*). Surprisingly, participants were *anti-Bayesian*, using their priors *less* with increasing noise. Continuous judgments of target displacement, however, did yield Bayesian behavior (*Experiment 3*) as found previously in other systems. We followed up on the unexpected categorical task results using macaques to allow for more precise eye movement monitoring and extensive within-subject testing. We analyzed prior use separately for sensory uncertainty added to the external image (*Experiment 4*) or caused by self-movement (*Experiment 5*). The monkeys were anti-Bayesian for image noise, like the humans, but Bayesian in compensating for motor-induced noise. A Discriminative learning-based model provided a feasible explanation for the anti-Bayesian results.

## MATERIALS AND METHODS

84 We have split Materials and Methods into 2 sections, *Experimental Design and Statistical*  
85 *Analyses and Modeling*. The *Experimental Design and Statistical Analyses* section has 3 sub-  
86 sections. Sub-section 1 includes the methods for the psychophysics experiments run on

87 humans. This includes an initial experiment to identify a sensory noise manipulation  
88 (Experiment 1), an experiment testing the trade-off between categorical priors and sensory  
89 uncertainty (Experiment 2), and an experiment testing the trade-off between continuous priors  
90 and sensory uncertainty (Experiment 3). Sub-section 2 details the methods for the experiments  
91 run on rhesus macaques. This sub-section includes the experiment to isolate the trade-off  
92 between a categorical prior and visual uncertainty alone (Experiment 4), between a categorical  
93 prior and motor uncertainty alone (Experiment 5), and a control experiment. Sub-section 3  
94 includes a description of the data preparation and analysis measures used throughout the  
95 manuscript. The *Modeling* section includes a detailed description of the computational models  
96 used in the manuscript.

## 97 **Section 1: Experimental Design and Statistical Analyses**

### 98 ***Sub-section 1. Human Psychophysics***

#### 99 Materials and paradigm

100 Forty-five adult volunteers with normal or corrected-to-normal vision participated in the  
101 experiments. All procedures were explained verbally to participants beforehand and written,  
102 informed consent was obtained. Participants were paid \$12/hr and informed that participation  
103 was completely voluntary. All procedures were performed in accordance with protocols  
104 approved by the Duke University Institutional Review Board.

105 Participants sat alone in a darkened room in front of a monitor with their head stabilized  
106 using a chin- and forehead-rest. The monitor was positioned at 60cm from the center of the  
107 head. Experiments 1 and 2 were displayed on a CRT monitor (Accusync 120) at 120Hz.  
108 Experiment 3 was displayed on a Dell LCD monitor at 60Hz. The experiment was written in and  
109 displayed using Presentation (Neurobehavioral systems, Albany, CA). Monocular eye position  
110 was recorded with an eye-tracking system developed by Matsuda et al. (2017).

111 Participants performed a modified Saccadic Suppression of Displacement task  
112 (Bridgeman et al., 1975) (Figure 1b; center panels). On each trial, a fixation cross first appeared  
113 near the center of the screen. Once participants acquired and maintained fixation for 500ms, a  
114 saccade target appeared at one of two average positions relative to the center of the screen:  
115 10° or -10°. A target at 10° appeared in the right half of the screen while a target at -10° appeared  
116 in the left half of the screen. Additionally, on every trial, the position of the target and fixation  
117 cross were both jittered by -0.5 to 0.5 degrees relative to the average position to mitigate the  
118 confounding effects of adaptation to either a constant saccade amplitude or a constant distance  
119 between the target and the edge of the screen. The fixation cross then disappeared for 500ms,  
120 and an auditory cue was presented to signal to participants that they were allowed to make a  
121 saccade to the target. If fixation was broken before the auditory cue, the trial was aborted and a  
122 new one began immediately. Saccade initiation (defined as the time the eye left a window of 2  
123 deg. relative to the fixation cross) triggered target displacement. In Experiments 1 and 2,  
124 participants provided a binary report on whether they had perceived the target as having moved  
125 or not. The target remained on the screen for 500ms after it was displaced, after which it was  
126 replaced by a response prompt screen (5 = moved, 0 = remained stationary). In these  
127 experiments, target displacement was drawn from overlapping Gaussian distributions  
128 designated as the “movement” and “non-movement” distributions. On trials where the target  
129 moved, the displacement was drawn from a relatively broad Gaussian distribution centered  
130 around 0 ( $\mu = 0^\circ$ ,  $\sigma = 1.5^\circ$ ). On “no movement” trials, the displacement was drawn from a very  
131 narrow Gaussian distribution centered around 0 ( $\mu = 0^\circ$ ,  $\sigma = 0.017^\circ$ ). A positive displacement  
132 meant that the target moved rightward, and a negative displacement meant it moved leftward.

133 In Experiment 3, participants provided a continuous report of the target’s postsaccadic  
134 location. For this study, the target stayed visible for 100ms after displacement and was then  
135 replaced by a screen where the mouse cursor (shaped “+”) was placed at the center of the

136 screen and restricted to the horizontal meridian. Participants could then move the mouse cursor  
137 to where they perceived the target as having landed.

138

139 Experiment 1: Testing stimuli for the sensory uncertainty manipulation

140 Throughout the study we manipulated priors and sensory noise. Our approach to manipulating  
141 priors was based on a previously established procedure (Rao et al., 2016). There are many  
142 potential ways to introduce sensory noise, however, and it was unclear which would be the best  
143 method for our goal of parametrically obscuring the detection of image movement. Experiment 1  
144 evaluated several options to achieve this goal. Nine human participants completed at least 100  
145 trials each in 8 experimental conditions: 4 candidate noise-manipulation stimuli at two  
146 uncertainty levels each. The probability of target movement across all stimulus conditions was  
147 0.5.

148

149 The 4 possible noise-manipulation stimuli were:

150 1) Arrow targets ( $1^\circ$  long with  $0.5^\circ$  width) that pointed either in the direction of their movement  
151 (congruent) or in the opposite direction (incongruent). The prediction was that incongruent  
152 movements (opposite to the direction indicated by the arrow) would induce greater uncertainty  
153 and decrease discriminability.

154 2) Targets consisting of a Gaussian cloud of 20 white squares ( $0.25^\circ \times 0.25^\circ$ ) for which the  
155 uncertainty corresponded to the standard deviation of the cloud (low uncertainty =  $0.063^\circ$  and  
156 high uncertainty =  $0.25^\circ$ ).

157 3) Targets consisting of squares ( $0.5^\circ \times 0.5^\circ$ ) at two levels of contrast (low uncertainty = 0.78  
158 and high uncertainty = 0.29).

159 4) Targets that were Gaussian “blobs” (isoluminant, Gaussian distributions of light) for which  
160 uncertainty corresponded to the standard deviation of the blob (low uncertainty = 0.19° and high  
161 uncertainty = 0.47°).

162

163 The outcome of this experiment determined how we manipulated the sensory uncertainty in the  
164 rest of the experiments.

165

166 Experiment 2: Trade-off between binary prior and sensory uncertainty in humans

167 We trained participants on the prior, cued by the color of the fixation cross, using performance-  
168 based feedback. They were told whether their responses were correct or incorrect on each trial  
169 using an image of a smiling or frowning face, respectively. Based on the results from  
170 Experiment 1, we chose the isoluminant Gaussian blob as sensory uncertainty manipulation  
171 (Figure 1b). The target was grayscale on every trial; only its width given by the standard  
172 deviation changed. The target had one of three possible standard deviations for the whole  
173 experiment – 0.1 deg. (“low noise”), 0.25 deg. (“medium noise”) or 0.5 deg. (“high noise”).

174 Twenty participants completed a total of 1300 trials each. Trials were presented in 100-  
175 trial blocks. For all participants, the first block was a baseline block where the color of the  
176 fixation cross was white, and the target moved on 50% of the trials. In the next 6 blocks, the  
177 fixation cross was either green or red, and vice versa for last 6. Each of these fixation colors  
178 was associated with one of two probabilities of target movement (0.9 or 0.1). The order of the  
179 two prior conditions and color-probability associations were counterbalanced across  
180 participants. As in Experiment 1, displacements were drawn from a relatively broad Gaussian  
181 distribution ( $\mu=0^\circ$ ,  $\sigma=1.5^\circ$ ) on “movement” trials and from a narrow Gaussian distribution ( $\mu=0^\circ$ ,  
182  $\sigma=0.017^\circ$ ) on “non-movement” trials to ensure that the solution to the task was probabilistic.  
183 Thus, the optimal solution to the task was to learn the probability that any given displacement  
184 was drawn from the “movement” distribution relative to the “non-movement” distribution. In

185 conditions with a biased prior (0.9 or 0.1), the optimal solution would be to weight this relative  
186 probability by the appropriate prior (detailed mathematical description in *Methods, Section 2:*  
187 *Modeling*). In other words, the optimal solution to this task is the Bayesian solution.

188 For 70% of the trials in blocks 2-13, the target had the lowest noise (standard deviation  
189 of 0.1°) and the probability of target displacement conformed to the experimental prior, i.e. 0.9  
190 or 0.1. These 70% of the trials were considered “training trials” where the intended prior was  
191 reinforced and maintained. The other 30% of trials were “testing trials”, where we tested the  
192 hypothesis that participants would use their learned prior more when the evidence was relatively  
193 uncertain. On these trials, the target had either medium or high sensory noise. Additionally, both  
194 to isolate the effects of a learned, color-associated expectation on performance and to mitigate  
195 the possibility that our sensory manipulation affected participants’ representation of the prior, the  
196 testing trials comprised a neutral condition where the target had a 0.5 probability of moving, but  
197 the fixation color cuing the prior was the same as the rest of the block. Training and testing trials  
198 were randomly interleaved (Figure 1c). To preserve a sense of experiential continuity across the  
199 experiment, 5% of the targets in block 1 had a standard deviation of 0.25 deg. (“medium-noise”)  
200 and 5% had a standard deviation of 0.5 deg. (“high-noise”). Data from these trials were not  
201 analyzed.

202

203 Experiment 3: Trade-off between continuous prior and sensory uncertainty in human  
204 participants

205 Fourteen human volunteers participated in Experiment 3. We tested the hypothesis that the  
206 visual system uses Bayesian inference to determine the *continuous* displacement value of  
207 objects across saccades. The overall paradigm was similar to Experiments 1 and 2. The critical  
208 difference was that the target was displayed post-saccadically for a limited period (100ms) and  
209 participants provided a continuous report of where they had perceived it as having landed.  
210 Participants fixated a central cross and upon being cued, made a saccade to a target located at

211 either 10° or -10°. The target was displaced horizontally during the saccade, displayed in its new  
212 location for 50ms, and then replaced by a response screen. The response screen consisted of a  
213 mouse cursor that started out in the center and was restricted to the horizontal meridian to  
214 ensure that participants were solving a one-dimensional problem. Participants were required to  
215 drag the mouse cursor to the location where the target had landed and click to submit their  
216 response.

217 Participants completed a total of 1000 trials each. We first trained participants on the  
218 prior for 600 trials and then tested the use of this prior with increasing sensory noise. As in  
219 Experiments 1 and 2, the target was a Gaussian blob and we manipulated sensory uncertainty  
220 by varying its width. The prior was a *continuous* Gaussian distribution of displacements, rather  
221 than a categorical prior indicating the probability of object displacement. Throughout the  
222 experiment, displacements were drawn from a Gaussian distribution with mean 0° and standard  
223 deviation 1°. Participants were trained on this prior in the first 600 trials with performance-based  
224 feedback. After they submitted their response, the target appeared in its correct postsaccadic  
225 location for 500ms. To indicate their degree of correctness, the color of this feedback target  
226 ranged continuously from green (correct) to red (incorrect by more than 2°). Targets in this  
227 training phase trials had a standard deviation of 0.1° (“low noise”).

228 In the remaining 400 trials, participants underwent a “testing” trials phase they were  
229 provided no feedback. These trials had one of 3 noise levels: 0.1° (“low noise”), 0.5° (“medium  
230 noise”), and 1° (“high noise”). Further, throughout the experiment, in 20% of the trials, the target  
231 did not appear post-saccadically. We call these “infinite noise” trials. All 4 noise levels were  
232 randomly interleaved throughout the testing phase. All data shown come from the testing phase  
233 of the experiment. We used participants’ performance in the infinite noise condition to evaluate  
234 how well they learned the prior in the training phase.

235

236 **Sub-section 2. Rhesus Macaque Psychophysics**

237 Materials and paradigm

238 Two rhesus macaques (Monkey S and Monkey T, both males) were trained to perform a  
239 modified Saccadic Suppression of Displacement paradigm, similar to the human participants.  
240 Animals were brought into the lab in custom-made chairs (Crist Instruments, Hagerstown, MD)  
241 and their heads were stabilized using a head-post that attached to both the chair and a  
242 surgically implanted socket (Crist Instruments, Hagerstown, MD) on the skull. The socket was  
243 implanted in an aseptic surgical procedure with the help of ceramic screws and acrylic. Eye  
244 position was measured using a surgically implanted scleral search coil (Robinson, 1963; Judge  
245 et al., 1980) in one eye. All surgical and experimental procedures were performed in  
246 accordance with protocols approved by the Duke Institutional Animal Care and Use Committee.

247 In a typical experimental session, the animals performed the behavioral task in a dark  
248 experimental rig. They were positioned 60cm from an LCD monitor (1920 x 1080, 144Hz). To  
249 dissociate external sources of sensory noise from internal, motor-driven sources, the saccade  
250 target was dissociated from a visual probe (a Gaussian blob) which was displaced  
251 intrasaccadically on some trials. In the human experiments, the Gaussian, visual probe (same  
252 as the saccade target) always appeared in one of two locations on the screen and only moved  
253 horizontally. For Experiments 4 and 5 in monkeys, it could appear in one of 4 locations,  $\pm 10^\circ$   
254 horizontally or  $\pm 10^\circ$  vertically. The saccade target was always positioned along the orthogonal  
255 cardinal direction (e.g. if the probe appeared at  $\pm 10^\circ$  horizontally, the saccade target would be  
256 at  $\pm 10^\circ$  vertically), and the probe was displaced in a direction parallel to the saccade vector. For  
257 the control experiment (with results presented in Figure 4h, i), we simultaneously recorded from  
258 neurons while the animals performed the sessions (neural data not presented in this  
259 manuscript). Since we placed the probe within the mapped receptive field of the neuron, the  
260 probe appeared in a different location during each session.

261 On each trial, a fixation square ( $1^{\circ} \times 1^{\circ}$ ) first appeared at the center of the screen. After  
262 fixation had been acquired and maintained for a randomized duration of 300-500ms, the visual  
263 probe appeared at one of the 4 locations on the screen for 500-700ms. The monkey was  
264 required to maintain fixation on the central fixation square for that duration, after which the  
265 fixation square was replaced by the saccade target ( $1^{\circ} \times 1^{\circ}$ ) indicating to the animal they could  
266 make a saccade. Saccade initiation (defined as the time the eye crossed a threshold set at 20%  
267 of the saccade length, i.e.,  $2^{\circ}$ , in the direction of the saccade) triggered the displacement of the  
268 probe on some trials. The probe was displaced in a direction parallel to the saccade. Animals  
269 were further required to maintain postsaccadic fixation for 700ms after which the saccade target  
270 was replaced by a white cross in the same location. To report that the probe had moved during  
271 the saccade, the monkey was required to make a saccade to the probe within 500ms and then  
272 fixate on it for 400ms. To report that it had remained stationary during the saccade, the monkey  
273 had to remain fixated on the cross for 1000ms. The precise timing of stimulus presentation was  
274 verified with a photodiode taped to the top left corner of the monitor, where a white square  
275 (invisible to the monkey) was flashed within the same frame as the measured stimulus.

276 Displacements were drawn from relatively broad and narrow Gaussian distributions in  
277 the movement ( $\mu = 0^{\circ}$ ,  $\sigma = 2.5^{\circ}$ ) and non-movement ( $\mu = 0^{\circ}$ ,  $\sigma = 0.2^{\circ}$ ) conditions, respectively.  
278 Positive displacements were either rightward or upward, and negative displacements were  
279 leftward or downward. Priors were cued by the color of the fixation and target squares. For  
280 monkey S, green squares meant that the probe had a 0.2 probability of being displaced while  
281 magenta squares indicated a 0.8 probability of displacement. For monkey T, blue squares were  
282 associated with a 0.2 probability of displacement while orange squares were associated with a  
283 0.8 probability of displacement. Animals were trained on priors over multiple sessions using  
284 performance-based feedback like human participants.

285 Experiment 4: Trade-off between categorical priors and visually-driven sensory uncertainty

286 To measure performance as a function of external sensory uncertainty, the visual probe in  
287 Experiment 4 was a Gaussian “blob” with one of three possible standard deviations: 0.5° (“low  
288 noise”), 1.25° (“medium noise”), and 2° (“high noise”) for Monkey S and 0.5° (“low noise”), 1.25°  
289 (“medium noise”), and 1.75° (“high noise”), for Monkey T. The relative frequencies of all trial 7  
290 types (2 priors x 3 noise levels + baseline) were the same as in the categorical experiment for  
291 humans (Experiment 2). Baseline trials with white squares and 0.5 probability of displacement  
292 all had “no noise” visual probes. In the 0.2 and 0.8 prior conditions, 70% of trials had no noise  
293 and conformed to the displacement probability indicated by the prior. The remaining 30% of  
294 trials with low and high noise comprised a neutral “test” condition with a veridical jump  
295 probability of 0.5. All 7 trial types were randomly interleaved.

296

297 Control experiment with valid prior statistics for all noise levels

298 We also performed a control experiment, the purpose of which was to determine if the anti-  
299 Bayesian results might be an artifact of adapting to the 0.5 probability of target movement in the  
300 medium- and high-noise conditions and ignoring the learned priors. In this experiment, the  
301 probability of movement matched the prior, e.g. 0.8 or 0.2, for all noise levels. Visual noise  
302 levels were manipulated the same as in Experiment 4.

303

304 Experiment 5: Trade-off between categorical priors and *motor-driven* sensory uncertainty

305 To measure performance as a function of internal, motor-driven sensory uncertainty, we added  
306 a condition to the experiment where monkeys did not make a saccade. The purpose was to  
307 eliminate a major form of saccade-driven sensory uncertainty, the saccadic suppression of  
308 visual signals. The monkeys remained fixated in the center while the Gaussian, visual probe  
309 was displaced. This no-saccade condition served as the “low motor noise” condition and was  
310 compared to a “high motor noise” condition where animals made a saccade. The temporal

311 structure of the no-saccade trials was identical to the trials with a saccade. No-saccade trials  
312 were implemented by assigning the location of the “saccade target” to be the same as the  
313 fixation square. There were three prior conditions: 0.2, 0.5, and 0.8. Colors indicating the priors  
314 were the same as in Experiment 4. The visual probe had a standard deviation of 0.5°, the lowest  
315 noise condition, for all trials. All 6 trial types (3 priors x 2 noise levels) were randomly  
316 interleaved.

317 ***Sub-section 3. Data Preparation and Analysis Measures***

318 Data preparation

319 Data from individual trials were analyzed offline to confirm that the visual probe landed in its  
320 displaced location before the end of the saccade. The saccade end time was defined as the  
321 time at which the eye velocity dropped below 0.04°/ms. For human participants, the time at  
322 which the target jump command was sent was recorded for each trial. Trials with a recorded  
323 jump time greater than 1 whole frame (8.33ms for Experiments 1 and 2, and 16.7ms for  
324 Experiment 3) before the detected end of the saccade were excluded from analysis. Participants  
325 for whom at least 90% of all trials did not meet this criterion were excluded from analyses  
326 entirely. No participants were excluded in Experiment 1, three participants were excluded from  
327 Experiment 2, and three participants were excluded from Experiment 3. For the macaque  
328 experiments, we used a photodiode to verify the exact timing of stimulus presentation. Note that  
329 the timestamp from the photodiode indicated the presentation of a white square at the top left of  
330 the screen and the monitor refreshes frames as a raster. We verified the maximum duration of a  
331 frame as being 7ms from top left to bottom right using a second photodiode. Since the probe  
332 was presented at various locations on the screen, we set the most conservative criterion such  
333 that the photodiode timestamp had to be at least 7ms before the detected end of the saccade.  
334 Individual trials that did not meet this criterion (less than 10% of trials across all sessions) in the  
335 macaque data were excluded as well.

336

337 Psychometric curves and prior use

338 All data were analyzed using MATLAB (Mathworks, Inc.). For Experiments 1, 2, 4, and 5,  
339 psychometric curves were fit to binary responses using the 4-parameter logistic regression  
340 model,

341

342

$$y = \max + \frac{\min - \max}{1 + \left(\frac{x}{\text{thresh}}\right)^{\text{slope}}} \quad (1)$$

343

344 where  $x$  is the absolute value of the presented displacement,  $y$  is the value of the psychometric  
345 function,  $\min$  is the minimum value of the function (i.e.,  $y$  at  $x = 0$ ),  $\max$  is the maximum value,  
346  $\text{thresh}$  is the inflection point, and  $\text{slope}$  is the slope of the psychometric function.  $\min$ ,  $\max$ ,  
347  $\text{thresh}$ , and  $\text{slope}$  terms were fit to binary data by minimizing mean squared error.

348 For all analyses in the main manuscript, we used the intercept of the psychometric curve  
349 as a measure of prior use in these experiments for statistical tests, and for comparison with the  
350 predictions of the categorical Bayesian model. For human participants and in the low-noise,  
351 prior training trials for macaques, displacements were drawn from continuous distributions. In  
352 these conditions, we used the value of  $\min$  as the intercept. For the medium and high noise  
353 hypothesis testing trials in macaques, displacements were discretized. There was a  
354 displacement = 0 condition. In these conditions, the intercept is simply the proportion of “moved”  
355 responses in the displacement = 0 condition.

356 We repeated all the analyses of prior use presented in the manuscript using a measure  
357 from Signal Detection Theory (Green and Swets, 1966), the Criterion. Criterion provides an  
358 alternative measure of bias in responses (i.e., a translational shift in psychometric curves). It is  
359 given by,

360                    $C = -0.5 (Z(\text{hit rate}) + Z(\text{false alarm rate}))$                    (2)

361 where the hit rate is the proportion of “jumped” responses on trials in which the probe truly  
362 moved, and the false alarm rate is the proportion of “jumped” responses on trials in which the  
363 probe did not move. The results using Criterion (not reported here) replicate the findings in the  
364 main manuscript.

365                  For all statistical comparisons, the assumption of normality was first tested for each  
366 sample using a Kolmogorov-Smirnov (KS) test. If met, we then used a parametric comparison  
367 such as an ANOVA or a t-test. Otherwise, the equivalent non-parametric test was used.

368

369 **Section 2: Modeling**

370 Categorical Bayesian ideal observer model

371 The results in Experiments 2, 4, and 5 were compared to the performance of a Bayesian ideal  
372 observer model in the categorical task. This section provides a detailed mathematical  
373 description of the model. A brief overview of the model and its key equations are also discussed  
374 in the text accompanying Figure 3 in the *Results*.

375                  The ideal observer makes a probabilistic decision about binary variable,  $J$ , indicating  
376 whether the target jumped or not.  $\neg J$  indicates that the target did not jump. Since the true  
377 displacement is experimentally drawn but not available to the observer, they make this decision  
378 given the *perceived* displacement,  $\hat{x}$ . The decision is based on the relative probabilities of the  
379 target having jumped or not jumped given the perceived displacement,

380                    $D(\hat{x}) = \mathbb{I}\{P(J|\hat{x}) > P(\neg J|\hat{x})\}$                    (3)

381 where  $D(\hat{x})$  is the decision given the perceived displacement,  $\hat{x}$ , and is determined by a binary  
382 indicator function,  $\mathbb{I}$ .  $\mathbb{I} = 0$  (no jump) if the condition in braces is not met. Otherwise,  $\mathbb{I} = 1$   
383 (jumped);  $P(J|\hat{x})$  is the probability that the probe jumped given  $\hat{x}$ ;  $P(\neg J|\hat{x})$  is the probability that  
384 the probe did not jump given  $\hat{x}$ .

385 Using Bayes' rule for the condition within braces in Eq. 3,

386

$$D(\hat{x}) = \mathbb{I} \left\{ \frac{P(\hat{x}|J)P(J)}{P(\hat{x}|\neg J)(1-P(J))} > 1 \right\} \quad (4)$$

387 The simulated decision of the ideal observer, however, must be compared to the responses of  
388 participants. We do not have access to participants' perceived displacement, but instead can  
389 only infer their decision given the true experimental displacement,  $x$ . We assume that the  
390 perceived displacement is a Gaussian random variable where the mean is the true  
391 displacement, and its variance given by the width of the blob on that trial:

392

$$\hat{x} \sim N(x, \sigma_t^2) \quad (5)$$

393 where  $\sigma_t$  is the variance of the target.

394 The decision given the true displacement can thus be modeled as,

395

$$D(x) = \int \mathbb{I} \left\{ \frac{P(\hat{x}|J)P(J)}{P(\hat{x}|\neg J)(1-P(\neg J))} > 1 \right\} P(\hat{x}|x) dx \quad (6)$$

396 That is, the decision value given the true displacement,  $D(x)$ , is the integral of the perceived  
397 displacement distribution that falls above the point at which the indicator function,  $\mathbb{I}$ , is non-zero.

398 Based on the distributions used in the experiment,

399

$$x|J \sim N(0, \sigma_J^2) \quad (7)$$

400 and

401

$$x|\neg J \sim N(0, \sigma_{\neg J}^2) \quad (8)$$

402 Since  $P(\hat{x}|x)$ ,  $P(x|J)$ , and  $P(x|\neg J)$  are all Gaussian distributions, we can integrate over  $x$  such  
403 that,

404

$$\hat{x}|J \sim N(0, \sigma_J^2 + \sigma_t^2) \quad (9)$$

405 and

406  $\hat{x}|\neg J \sim N(0, \sigma_{\neg J}^2 + \sigma_t^2)$  (10)

407 Thus, the expression inside the indicator function in Eq. 6, when replaced with the appropriate  
 408 Gaussian probability density functions, equals,

409 
$$\frac{\frac{1}{\sqrt{(\sigma_J^2 + \sigma_t^2)2\pi}} e^{-\frac{1}{2}\left(\frac{(\hat{x}-0)^2}{\sigma_J^2 + \sigma_t^2}\right)} P(J)}{\frac{1}{\sqrt{(\sigma_{\neg J}^2 + \sigma_t^2)2\pi}} e^{-\frac{1}{2}\left(\frac{(\hat{x}-0)^2}{\sigma_{\neg J}^2 + \sigma_t^2}\right)} (P(\neg J))} > 1 \quad (11)$$

410 Taking the log on both sides provides the condition under which the indicator function is greater  
 411 than 0,

412 
$$\log\left(\frac{\frac{1}{\sqrt{(\sigma_J^2 + \sigma_t^2)2\pi}} e^{-\frac{1}{2}\left(\frac{(\hat{x}-0)^2}{\sigma_J^2 + \sigma_t^2}\right)} P(J)}{\frac{1}{\sqrt{(\sigma_{\neg J}^2 + \sigma_t^2)2\pi}} e^{-\frac{1}{2}\left(\frac{(\hat{x}-0)^2}{\sigma_{\neg J}^2 + \sigma_t^2}\right)} (P(\neg J))}\right) > \log(1) = 0 \quad (12)$$

413 That is,

414 
$$\log\left(\frac{1}{\sqrt{(\sigma_J^2 + \sigma_t^2)2\pi}} e^{-\frac{1}{2}\left(\frac{(\hat{x}-0)^2}{\sigma_J^2 + \sigma_t^2}\right)} P(J)\right) - \log\left(\frac{1}{\sqrt{(\sigma_{\neg J}^2 + \sigma_t^2)2\pi}} e^{-\frac{1}{2}\left(\frac{(\hat{x}-0)^2}{\sigma_{\neg J}^2 + \sigma_t^2}\right)} P(\neg J)\right) > 0 \quad (13)$$

415

416 Rearranging terms to solve for  $\hat{x}^2$ , we find that the indicator function is  $> 0$  when  $\hat{x}^2$  is  
 417 greater than a criterion value,  $\hat{x}_C^2$ , defined as,

418 
$$\hat{x}^2 > \hat{x}_C^2 = \frac{\log\left(\frac{\sigma_J^2 + \sigma_t^2}{\sigma_{\neg J}^2 + \sigma_t^2}\right) + 2 \log \frac{P(\neg J)}{P(J)}}{\frac{1}{\sigma_{\neg J}^2 + \sigma_t^2} - \frac{1}{\sigma_J^2 + \sigma_t^2}} \quad (14)$$

419 Since  $\hat{x}$  is a Gaussian random variable,  $\hat{x} \sim N(x, \sigma_t^2)$ ,  $\frac{\hat{x}^2}{\sigma_t^2}$  is a non-central chi-square random

420 variable,  $\frac{\hat{x}^2}{\sigma_t^2} \sim X^2 \left(1, \frac{x^2}{\sigma_t^2}\right)$ . Thus, the decision,  $D(x)$ , can be modeled as the integral of a non-

421 central chi-square distribution that lies above the criterion,  $\hat{x}_C^2$ . That is,

422

$$D(x) = 1 - F_{X^2} \left( \frac{\hat{x}_C^2}{\sigma_t^2}, df = 1, \lambda = \frac{x^2}{\sigma_t^2} \right) \quad (15)$$

423 where  $F_{X^2}$  is the cumulative distribution function of  $X^2$  with degrees of freedom,  $df = 1$  and

424 gamma,  $\lambda = \frac{x^2}{\sigma_t^2}$  up to  $\frac{\hat{x}_C^2}{\sigma_t^2}$ .

425

#### 426 Continuous Bayesian model: Simulation and fitting

427 Results in Experiment 3 are compared to the performance of a Bayesian ideal observer for the

428 continuous task. The ideal observer infers the perceived displacement as a reliability-weighted

429 combination of the sensory likelihood and prior distributions,

430

$$D_{perceived} = w_{prior} D_{prior} + w_{likelihood} D_{likelihood} \quad (16)$$

431 where  $D_{perceived}$  is the mean of the inferred posterior distribution,  $w_{prior}$  is the weight assigned

432 to the prior,  $D_{prior}$  is the mean of the prior distribution,  $w_{likelihood}$  is the weight assigned to the

433 likelihood, and  $D_{likelihood}$  the likelihood distribution. When both  $D_{prior}$  and  $D_{likelihood}$  are

434 Gaussian distributions, the weight terms are given by,

435

$$w_{prior} = \frac{\sigma_{likelihood}^2}{\sigma_{likelihood}^2 + \sigma_{prior}^2} \quad (17)$$

436 and

437

$$w_{likelihood} = \frac{\sigma_{prior}^2}{\sigma_{likelihood}^2 + \sigma_{prior}^2} \quad (18)$$

438 That is, the more reliable (i.e., less variable) estimate is weighted higher. This reliability-  
439 weighted inference is additionally the Bayes optimal estimate because the variance of the  
440 estimate,  $\sigma_{perceived}^2$ , is lower than the variance of both the prior and the likelihood distributions:

441

$$\sigma_{perceived}^2 = \frac{1}{\frac{1}{\sigma_{likelihood}^2} + \frac{1}{\sigma_{prior}^2}} \quad (19)$$

442 We simulated the final response as the mean of the posterior distribution, i.e., its  
443 maximum value. The values of the parameters used to simulate ideal observer responses were  
444 the same as the ones used in the experiment. We then minimized squared error between each  
445 participant's responses and those of the Bayesian ideal observer model to identify the best-fit  
446 values for their internal prior and likelihood distributions. Best-fit parameters were identified on a  
447 participant-by-participant basis. Parameter optimization was performed using Matlab's *fmincon*  
448 function.

449

450 **RESULTS**

451 **Gaussian blurring induces uncertainty of image movement**

452 The premise of the study was that, if active visual perception were Bayesian, subjects would  
453 use priors more when sensory uncertainty increased. That is, the visual system would rely more  
454 on prior expectations about image movement if it was harder to detect the movement, in  
455 accordance with Bayesian ideal observer modeling. To train priors or cue learned priors, we  
456 used the color of the fixation cross (Figure 1b, top dashed box), similar to the method of Rao et  
457 al. (2016) in which the color of the target itself indicated the prior. Sensory uncertainty  
458 manipulations were a new addition to the paradigm, however, so to select a satisfactory  
459 approach we compared four potential methods to make image movement harder to detect, each

460 at two levels of increasing uncertainty (Experiment 1;  $n = 9$  human participants). The four  
 461 methods were to use 1) an arrow image that jumped either “congruently” in the direction in  
 462 which it pointed, thus having low sensory uncertainty, or incongruently, thus having high  
 463 uncertainty, 2) a Gaussian cloud image of white squares in which the noise corresponded to the  
 464 standard deviation of the cloud (low noise =  $0.0625^\circ$  and high noise =  $0.25^\circ$ ), 3) square images  
 465 at two contrast levels (low noise = 78.4% and high noise = 29.4%), and 4) isoluminant Gaussian  
 466 “blob” images in which the noise corresponded to the standard deviation of the blob (low noise =  
 467  $0.19^\circ$  and high noise =  $0.47^\circ$ ).

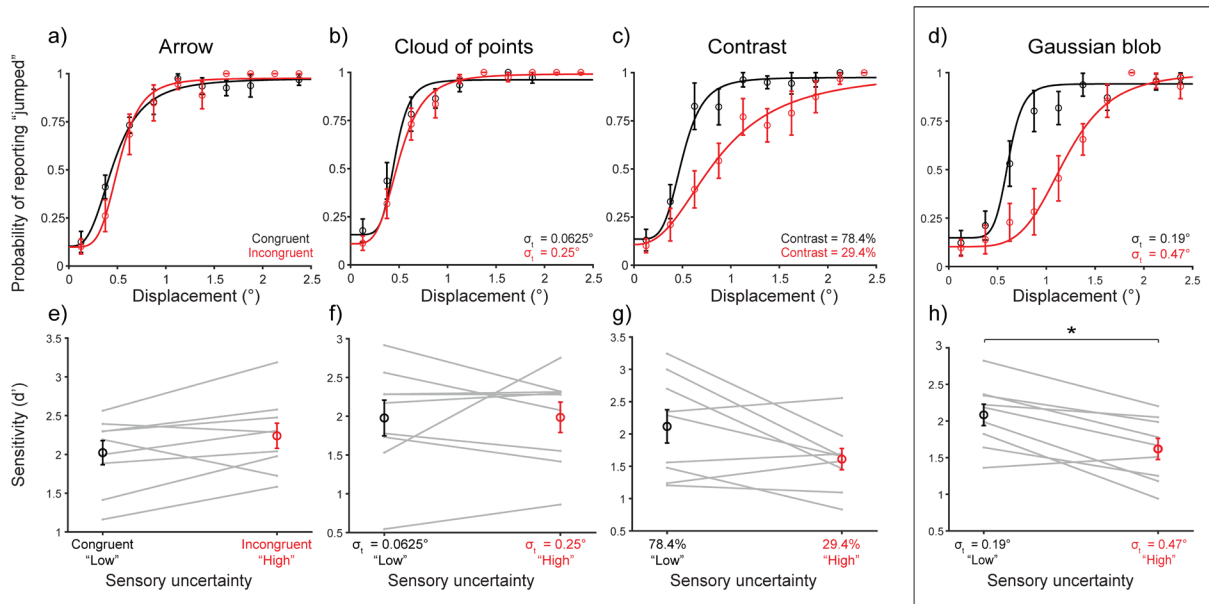


**Figure 2.** Results of Experiment 1. Top row shows psychometric curves in the low (black) and high (red) noise conditions. Bins averaged across participants. Error bars: S.E.M. Curves were fit to pooled data. Bottom row shows  $d'$  values in the two noise conditions. Gray lines: Individual participants. Markers and error bars: means and S.E.M across participants. a, e) congruent and incongruent arrow stimulus, b, f) Gaussian cloud of points, c, g) high and low contrast stimuli, d, h) Gaussian blob stimulus (emphasized by a gray box since it is the manipulation we selected to use for the rest of the experiments). \*,  $p < 0.0125$ .

468 For the arrow (Figure 2a, e) and Gaussian cloud (Figure 2b, f) manipulations,  
 469 psychometric curves (fit to pooled data across participants) did not change in steepness  
 470 between the low (black) and high noise (red) conditions. We also found no significant difference  
 471 in sensitivity, measured by  $d'$  (Green and Swets, 1966), between the low noise (mean = 2.02,

472 SE = 0.16 for arrow; mean = 1.98, SE = 0.23 for Gaussian cloud) and high noise (mean = 2.24,  
473 SE = 0.16 for arrow; mean = 1.99, SE = 0.20 for Gaussian cloud) conditions ( $p = 0.091$  and  $p =$   
474 0.97 for Gaussian cloud on a paired t-test).

475 For stimuli with different contrasts (Figure 2c, g), sensitivity in the low noise condition  
476 (mean = 2.12, SE = 0.16) trended higher than in the high noise condition (mean = 1.61, SE =  
477 0.16), but the difference was not statistically significant at  $n = 9$  participants ( $p = 0.055$  on a  
478 paired t-test). However, increasing the standard deviation of an isoluminant Gaussian “blob”  
479 target (Figure 2d,h; highlighted with a box) reliably induced sensory uncertainty. This  
480 manipulation yielded psychometric functions that were steeper in the lower-noise condition  
481 (Figure 2d, black curve,  $\sigma_t = 0.19^\circ$ ) than in the high-noise condition (Figure 2d, red curve,  $\sigma_t =$   
482  $0.47^\circ$ ). There were significant differences in sensitivity to target jumps, measured by  $d'$  (Green  
483 and Swets, 1966), between the low (mean = 2.08, SE = 0.15) and high (mean = 1.62, SE =  
484 0.14) noise levels ( $p = 0.0023$  on a paired t-test, Bonferroni corrected for four comparisons)  
485 (Figure 2h). Therefore, we chose Gaussian blobs of varying widths as the targets for the  
486 remaining experiments.

487 **Categorical judgments of displacement are anti-Bayesian**

488 In Experiment 2, we used a modified Saccadic Suppression of Displacement (SSD) task  
489 (Bridgeman et al., 1975) in which we manipulated priors and sensory noise (Figure 1b) to test  
490 the Bayesian hypothesis. Human participants fixated near the center of a screen, and upon  
491 being cued, made a saccade to a target. During the saccade, the target was displaced by  
492 varying amounts. After the saccade, participants reported their perception of whether the target  
493 had moved or not. Sensory uncertainty was induced by using Gaussian blob targets having  
494 widths ( $\sigma_t$ ) of  $\sigma_t = 0.1^\circ$  (low noise),  $\sigma_t = 0.25^\circ$  (medium noise), or  $\sigma_t = 0.5^\circ$  (high noise).  
495 Participants were trained on priors,  $P(J)$ , using performance-based feedback. Prior training trials  
496 constituted 70% of trials in each prior block (Figure 1c). The fixation color indicated  $P(J) = 0.1$  or

497 0.9 and the target had the lowest uncertainty, essentially punctate. The remaining 30% of trials  
498 were “hypothesis testing” trials. The color of the fixation cross indicated the prior, but the true  
499 jump probability was a neutral 0.5 to isolate the effects of the learned, color-cued priors. Targets  
500 in these trials had additional sensory uncertainty (“medium” or “high”). The hypothesis testing  
501 trials were relatively infrequent and interspersed randomly to mitigate the possibility of  
502 participants recognizing that higher noise targets implied a neutral prior. We also performed a  
503 control experiment in which the jump probability matched the priors across noise conditions, as  
504 described below.

### Bayesian predictions

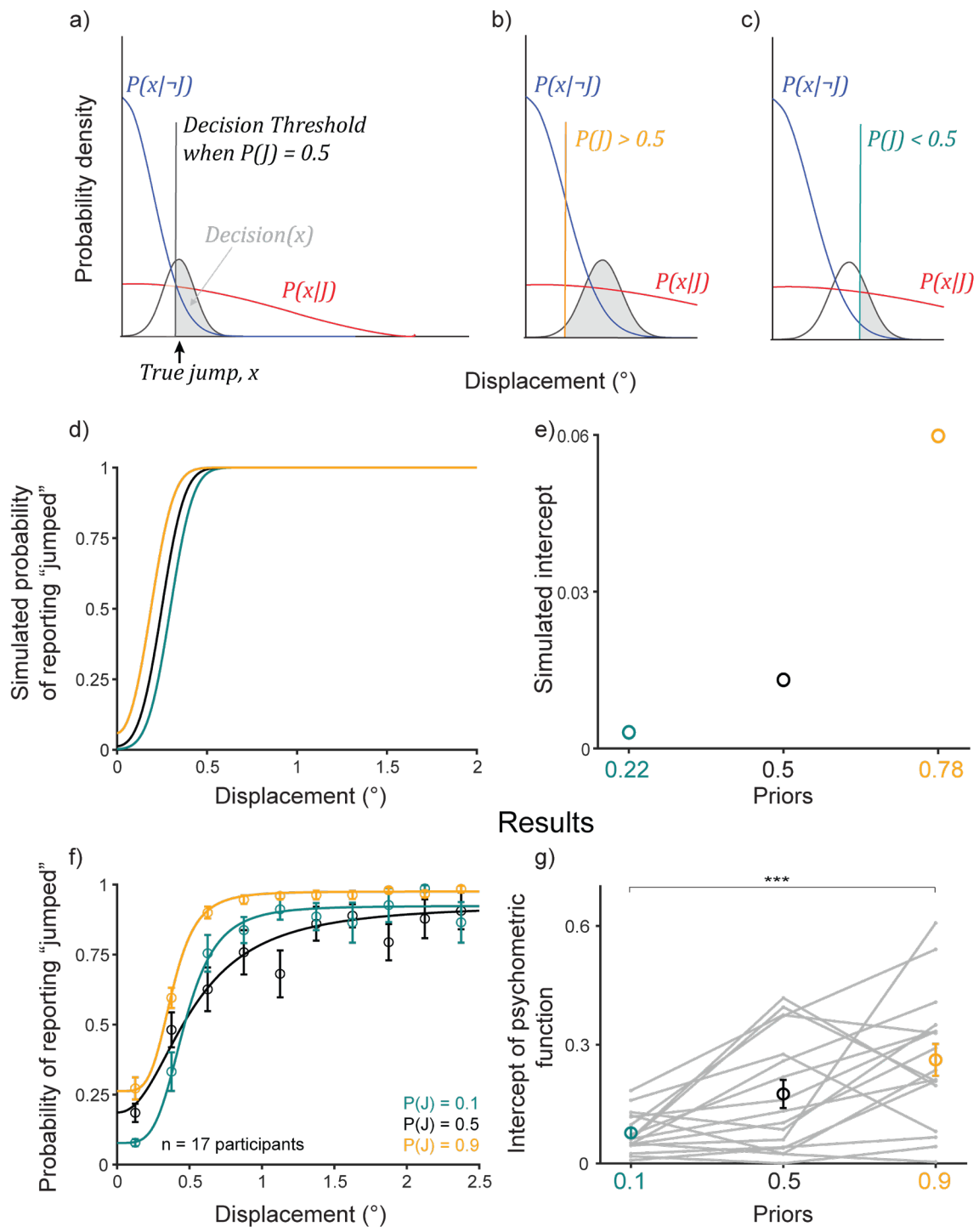


**Figure 3.** Participants learned the priors. a-c) Bayesian ideal observer models for the 3 prior conditions. d) Bayesian predictions for prior learning. e) Intercepts for curves in (d). f) Psychometric curves from  $n = 17$  participants. g) Intercepts for curves in (f), fit to individual participants, matched Bayesian predictions in (e). \*\*\*,  $p < .001$ .

505 To analyze data in Experiment 2, we compared participants' performance with the  
 506 predictions of a Bayesian ideal observer model (Figure 3a-c; details under *Methods, Section 2:*  
 507 *Modeling*). On every trial, the ideal observer decided whether the probe jumped or not given a  
 508 perceived displacement,  $\hat{x}$ . The decision would be "yes" if the probability of a jump given  $\hat{x}$ ,  
 509  $P(J|\hat{x})$ , exceeded the probability of non-jump given  $\hat{x}$ ,  $P(\neg J|\hat{x})$ :

$$510 \quad D(\hat{x}) = \mathbb{I}\{P(J|\hat{x}) > P(\neg J|\hat{x})\} \quad (20)$$

511 The decision variable  $D(\hat{x})$  is determined by a binary indicator function,  $\mathbb{I}$ .  $\mathbb{I} = 0$  (no jump) if the  
 512 condition in braces is not met. Otherwise,  $\mathbb{I} = 1$  (jumped). Using Bayes' rule,

$$513 \quad D(\hat{x}) = \mathbb{I}\{P(\hat{x}|J)P(J) > P(\hat{x}|\neg J)(1 - P(J))\} \quad (21)$$

514 where  $P(\hat{x}|J)$  and  $P(\hat{x}|\neg J)$  are the likelihoods of "jump" and "no jump," respectively. For each  
 515 prior,  $P(J)$ , there was a threshold at which the condition in braces was met, i.e., it was equally  
 516 likely that the probe jumped or did not. For  $P(J) = 0.5$ , it was where the two likelihood  
 517 distributions intersected and were equal (Figure 3a, black vertical line). If there was no sensory  
 518 uncertainty, i.e., if  $\hat{x} = x$  where  $x$  was the true displacement, the ideal observer would report "no  
 519 jump" for all displacements less than the threshold and "jump" for all displacements above the  
 520 threshold. Since the target was a Gaussian blob, we assume Gaussian uncertainty  $\sigma_t$ ,  
 521 determined by the target, about the true displacement,  $x$  (Figure 3a, black distribution):

$$522 \quad \hat{x} \sim N(x, \sigma_t) \quad (22)$$

523 Therefore, the decision given the true displacement,  $D(x)$ , was the integral over values of  $x$   
 524 greater than the decision threshold (Figure 3a, shaded region):

$$525 \quad D(x) = \int \mathbb{I}\left\{\frac{P(\hat{x}|J)P(J)}{P(\hat{x}|\neg J)(P(\neg J))} > 1\right\} P(\hat{x}|x) dx \quad (23)$$

526 This restricted the value of the decision to range from 0 to 1.

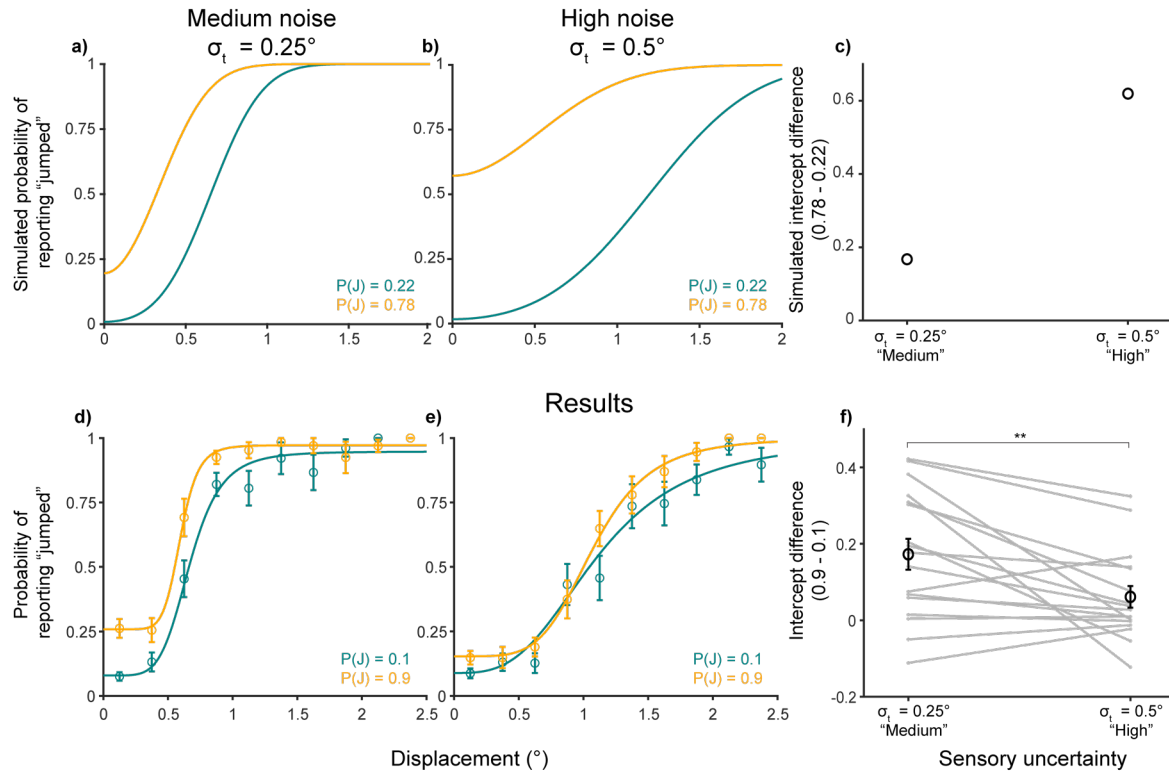
527 We first assessed prior learning. For a high prior, e.g.,  $P(J) = 0.9$ , the threshold would  
 528 move to the left since  $P(\hat{x}|J)$  was weighted higher than  $P(\hat{x}|\neg J)$ , thus increasing the ratio in the  
 529 braces (Figure 3b), and vice versa for a lower prior, e.g.  $P(J) = 0.1$  (Figure 3c). Critically, for the

530 same perceived displacement, the ideal observer was more likely to report that the probe  
531 jumped for a higher prior than for a lower prior. Figure 3d shows simulations for an ideal  
532 observer with likelihood distributions,  $P(\hat{x}|J) \sim N(0, 2)$  and  $P(\hat{x}|\neg J) \sim N(0, 0.017)$ , prior  $P(J) = 0.22$   
533 (teal),  $P(J) = 0.5$  (black), and  $P(J) = 0.78$  (orange), and sensory noise,  $\hat{x} \sim N(x, 0.1)$ . We chose  
534  $P(J) = 0.22$  and  $0.78$  for the simulations to account for 70% true-statistic trials and 30% neutral.  
535 The key point was that the high prior was  $>0.5$  and the low prior was  $<0.5$ . Figure 3e shows the  
536 value of the curves at displacement = 0 (the intercept).

537 For the human participants ( $n = 17$ , Figure 3f), in the prior *training* trials, psychometric  
538 curves shifted upward for the high prior (orange curve) and downward for the low prior (teal  
539 curve) at small displacements as predicted. The crossing of the low-prior (teal) curve over the  
540 black was not predicted but has implications that are addressed below (Figures 9-10 and their  
541 associated text). A lower intercept in the low prior condition than in the high prior condition  
542 (Figure 3g) matched the Bayesian predictions in Figure 3e. Repeated-measures ANOVA on the  
543 intercepts with prior as the within-conditions factor yielded a significant main effect of priors  
544 ( $F(2) = 11.82$ ;  $p = 0.0001$ ). Post-hoc comparison (Tukey HSD) of the  $P(J) = 0.9$  and  $0.1$   
545 conditions, the two priors tested later in hypothesis testing trials, showed that high-prior  
546 intercepts (mean =  $0.26$ , SE =  $0.04$ ) were significantly higher than low-prior intercepts (mean =  
547  $0.08$ , SE =  $0.01$ ;  $p = 2.79 \times 10^{-4}$ ). These results indicated that participants learned the priors as  
548 expected.

## Experiment 2: Hypothesis testing trials

### Bayesian predictions



### Control experiment for trial statistics

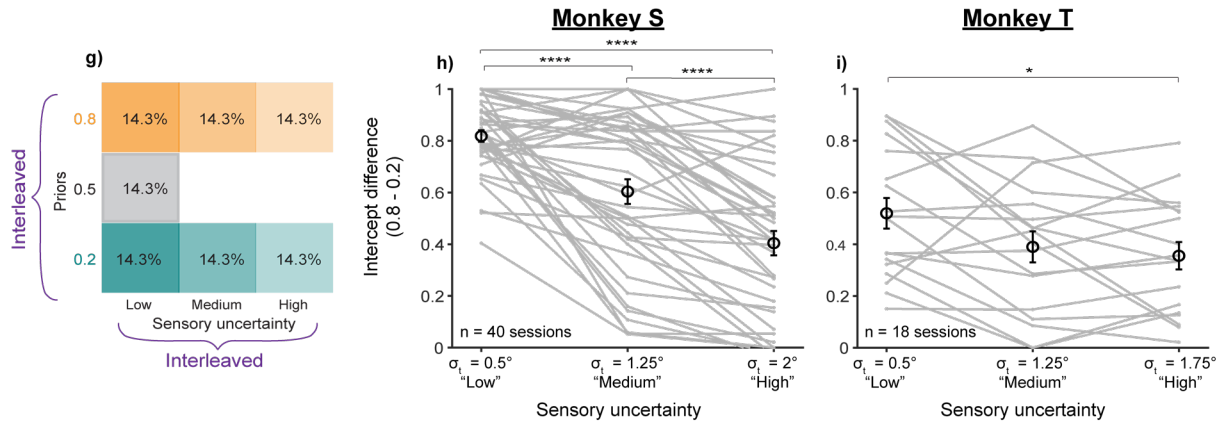


**Figure 4.** Categorical judgments of displacement are anti-Bayesian. **a-b)** Predicted psychometric curves from the Bayesian ideal observer model for the (a) medium and (b) high noise conditions. **c)** High-low prior intercept differences for the curves in a-b. **d-f)** Results from  $n = 17$  participants for the (d) medium and (e) high noise conditions, and (f) the respective high-low prior intercept differences. \*\*,  $p < 0.01$ . **g-h)** Results from a control experiment run on monkeys, in which the true jump probability matched the prior for the medium- and high-noise trials. **g)** Trial breakdown. **h-i)** High-low prior intercept difference ( $0.8 - 0.2$ ) across noise levels for (h) Monkey S and (i) Monkey T. \*\*\*\*,  $p < 0.0001$ ; \*,  $p < 0.05$ .

549 In the randomized, less frequent *hypothesis testing* trials, we tested the Bayesian  
550 hypothesis that priors are used more with increasing uncertainty. In these trials, the targets had  
551 medium or high sensory uncertainty. Figures 4a,b show Bayesian predictions for these medium-  
552 and high-noise conditions, respectively. We used the same likelihood ratios and priors as in  
553 Figure 3a-c, but with sensory noise  $\hat{x} \sim N(x, 0.25)$  and  $\hat{x} \sim N(x, 0.5)$ , respectively, to match the  
554 medium and high noise target widths. The model predicted greater separation between the low-  
555 (teal) and high-prior (orange) decision curves, i.e., greater prior use, in the high noise condition  
556 than in the medium noise condition, quantified by the high prior - low prior intercept difference  
557 (Figure 4c). In other words, the Bayesian ideal observer used the prior more with increasing  
558 sensory noise.

559 Human participants showed the opposite effect: they used their priors *less* with  
560 increasing noise. Psychometric curves across priors moved closer together in the high-noise ( $\sigma$   
561 =  $0.5^\circ$ ) condition (Figure 4e) compared to the medium-noise ( $\sigma = 0.25^\circ$ ) condition (Figure 4d).  
562 The difference in intercepts was significantly greater in the medium-noise condition (mean =  
563 0.17, SE = 0.04) than in the high-noise condition (mean = 0.06, SE = 0.03;  $p = 0.0081$  using a  
564 paired t-test) (Figure 4f). Overall, the results in Experiment 2 suggested that, in this sense,  
565 human participants were *anti-Bayesian*.

566 We considered the possibility that participants were not anti-Bayesian but had learned  
567 that trials with medium- and high-noise targets had a neutral jump probability. In this case, their  
568 prior for the hypothesis testing trials would be 0.5 and the Bayesian prediction is for the orange  
569 and teal psychometric curves to collapse together with increasing noise. Note that if the  
570 participants *only* learned the priors according to target type (i.e., low noise targets = color-cued  
571 prior, but medium and high noise targets = 0.5), then there would be no separation between the  
572 orange and teal psychometric curves at all. Therefore, participants clearly learned the color-  
573 associated priors. Nevertheless, to account for this potential confound, we analyzed results from  
574 a control experiment using two rhesus macaques in which the jump probability matched the

575 color-associated prior for *all* noise levels. A full description of the monkey experiments is  
576 provided in *Methods, Sub-section 2*. Briefly, all seven trial types (3 priors with low sensory noise  
577 + 2 each with medium and high noise) were randomly interleaved and had the same relative  
578 frequencies (Figure 4g). Consistent with the human results, the intercept differences between  
579 the  $P(J) = 0.8$  and  $0.2$  conditions *decreased* with increasing sensory noise (Figure 4h-i) for both  
580 monkeys. Repeated-measures ANOVA on intercept differences with noise levels as the main  
581 within-subjects factor yielded significant effects (Monkey S:  $F(2) = 51.75$ ,  $p = 4.97 \times 10^{-15}$ ;  
582 Monkey T:  $F(2) = 4.56$ ,  $p = 0.0176$ ). For monkey S ( $n = 40$  sessions), post-hoc comparisons  
583 (Tukey HSD) showed that intercept differences in the low noise condition ( $\sigma_t = 0.5^\circ$ ; mean =  
584  $0.82$ , SE =  $0.02$ ) were significantly higher than in the medium noise ( $\sigma_t = 1.25^\circ$ ; mean =  $0.60$ , SE  
585 =  $0.05$ ;  $p = 3.49 \times 10^{-6}$ ) and high noise ( $\sigma_t = 2^\circ$ ; mean =  $0.40$ , SE =  $0.05$ ;  $p = 0$ ) conditions.  
586 Intercept differences in the medium noise condition were also higher than in the high noise  
587 condition ( $p = 1.51 \times 10^{-5}$ ). For Monkey T ( $n = 18$  sessions), there was a significant difference  
588 between the low ( $\sigma_t = 0.5^\circ$ ; mean =  $0.52$ , SE =  $0.06$ ) and high noise ( $\sigma_t = 1.75^\circ$ ; mean =  $0.36$ , SE  
589 =  $0.05$ ;  $p = 0.0190$ ) conditions. Intercept differences in the medium noise condition ( $\sigma_t = 1.25^\circ$ ;  
590 mean =  $0.39$ , SE =  $0.06$ ) fell between the low and high noise conditions, not significantly  
591 different from either. Overall, the results replicated our human findings to confirm that the anti-  
592 Bayesian effect was based on learned, color-associated priors.

593

#### 594 **Continuous judgments of displacement are Bayesian**

595 Do the above results mean that the perception of visual displacement across saccades is  
596 always anti-Bayesian? Or was that outcome due, at least in part, to the categorical (binary)  
597 nature of the task? We tested this in Experiment 3 by requiring *continuous* estimates of  
598 displacement across saccades (Niemeier et al., 2003). Human participants performed the same  
599 SSD task, but instead of providing a binary report of “jumped” or “did not jump,” they provided a  
600 continuous report using a mouse cursor (Figure 5a). The target jumps were horizontal, and the

601 mouse cursor was restricted to that dimension. Formulating the task as a unidimensional,  
602 continuous problem allowed us to cast it in a form that has been tested across many  
603 sensorimotor domains (e.g., Jacobs 1999; Ernst and Banks, 2002; Kording and Wolpert, 2004;  
604 Fetsch et al., 2012; Darlington et al., 2017). If the uncertainty about the stimulus is modeled as  
605 the sensory likelihood, then the mean of the posterior (its maximum value and thus, our  
606 approximation of the inferred response) would be a reliability-weighted combination of the  
607 sensory likelihood and prior distributions (Figure 5b),

$$608 \quad \mu_{posterior} = \frac{\sigma_{likelihood}^2 \mu_{prior} + \sigma_{prior}^2 \mu_{likelihood}}{\sigma_{likelihood}^2 + \sigma_{prior}^2} \quad (24)$$

609 As  $\sigma_{likelihood}^2$  increases, with the other terms held constant,  $\mu_{posterior}$  approaches  $\mu_{prior}$ . In other  
610 words, for a given prior with fixed uncertainty, the response should get closer to the prior with  
611 greater sensory uncertainty.

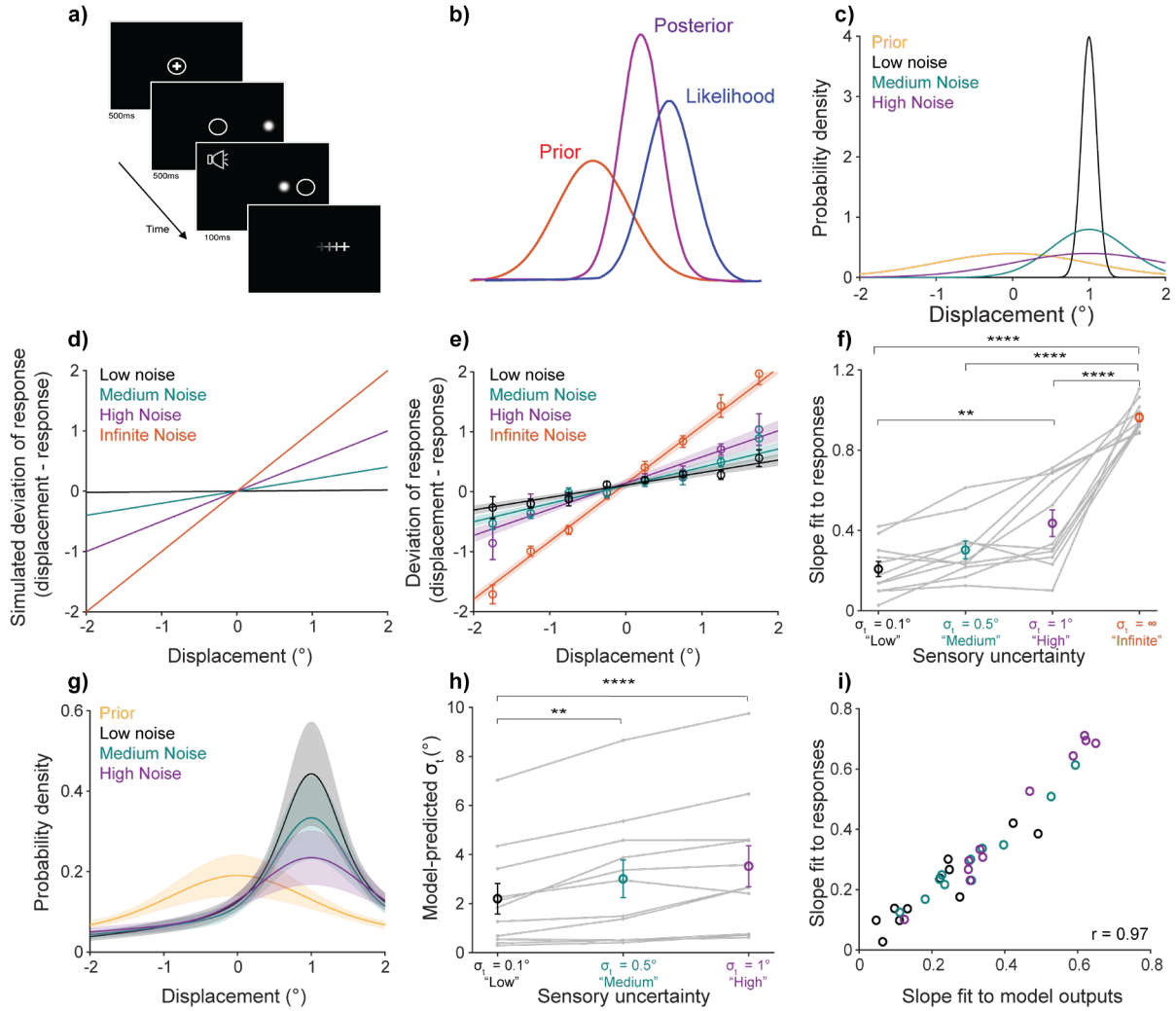


**Figure 5.** Continuous displacement perception is Bayesian. a) Task schematic. Participants performed the same SSD task as in Experiments 1 and 2 but provided a continuous estimate of where the target landed after the saccade using a mouse cursor (+). b) Bayesian inference for continuous stimulus estimation. c) Distributions used in the experiment. Distributions for the three noise levels are centered on displacement = 1° for illustration. d) Bayesian predictions for the experimental parameters in (c). e) Results from  $n = 11$  participants. Bins and lines, fit to individuals, were averaged across participants. Error bars and shaded regions: S.E.M. f) Slopes of lines in (e). g) Model fits for participants' internal prior and likelihood distributions, to be compared with (c). h) Standard deviations of likelihood distributions in (g). i) Correlation between model-predicted slopes computed in the same way as the slopes in (f) and the empirical slopes from (f) on a participant-by-participant basis. \*\*,  $p < 0.01$ ; \*\*\*\*,  $p < 0.0001$ .

612        The prior was a Gaussian statistical distribution with  $\mu_{\text{prior}} = 0^\circ$  and  $\sigma_{\text{prior}} = 1^\circ$ . Participants  
 613        were first trained on the prior for 600 trials using performance-based feedback. They then  
 614        performed 400 hypothesis testing trials that provided no feedback. There were four sensory  
 615        uncertainty conditions: low noise ( $\sigma_t = 0.1^\circ$ ), medium noise ( $\sigma_t = 0.5^\circ$ ), high noise ( $\sigma_t = 1^\circ$ ), and

616 an “infinite noise” condition in which the target did not reappear postsaccadically. Figure 5c  
617 illustrates the distributions used in the experiment, with the prior centered at 0° and the  
618 likelihood (Gaussian blob) distributions centered, for purpose of illustration, on displacement =  
619 1°.

620 Figure 5d shows the predicted deviation in response from the presented displacement  
621 (displacement - response) for a Bayesian ideal observer (details in *Methods, Section 2:*  
622 *Modeling*). If the sensory uncertainty is much smaller than that of the prior, as in the lowest  
623 noise condition (black line), then the deviation of the posterior (response) from the true  
624 displacement should be near 0 for all presented displacements. Conversely, for maximal  
625 sensory uncertainty as in the infinite noise condition (orange line), the response should always  
626 be the mean of the prior. Since  $\mu_{\text{prior}} = 0^\circ$ , the deviation for each displacement equals the  
627 displacement itself. The medium (teal) and high (purple) noise conditions are predicted to fall in  
628 between the low and infinite noise conditions, with slopes proportional to noise level. In  
629 summary, the slope of the deviation line increases with increasing sensory uncertainty.

630 Participants’ ( $n = 11$ ) responses in the hypothesis testing trials matched Bayesian  
631 predictions (Figure 5e). The slopes of the deviation lines increased with increasing sensory  
632 uncertainty (Figure 5f). Repeated-measures ANOVA on the slopes yielded a significant main  
633 effect of noise level ( $F(3) = 78.01$ ,  $p = 2.87 \times 10^{-11}$ ). Post-hoc comparison of conditions (Tukey  
634 HSD) showed that slopes in the low-noise ( $\sigma_t = 0.1^\circ$ ) condition (mean = 0.21, SE = 0.04) were  
635 significantly lower than in the high-noise ( $\sigma_t = 1^\circ$ ; mean = 0.44, SE = 0.07,  $p = 0.0011$ ) and  
636 infinite noise conditions (mean = 0.96, SE = 0.02;  $p = 6.98 \times 10^{-14}$ ). Also, slopes in the medium  
637 noise condition ( $\sigma_t = 0.5^\circ$ , mean = 0.30, SE = 0.04) were significantly lower than in the infinite  
638 noise condition ( $p = 2.05 \times 10^{-12}$ ), and slopes in the high-noise condition were significantly lower  
639 than in the infinite-noise condition ( $p = 4.65 \times 10^{-10}$ ).

640 We fit individual participant responses to a Bayesian ideal observer model by minimizing  
641 squared error to infer their used prior and sensory likelihood distributions (Figure 5g). The prior

642 mean and standard deviation, and standard deviations of the low-, medium- and high-noise  
643 parameters, were fit simultaneously by assuming that the response in the infinite noise condition  
644 was the prior mean. Model outputs for the prior mean (mean = 0.05, SE = 0.04) were not  
645 significantly different from 0, the true prior ( $p = 0.22$ , one-sample t-test). Fit parameters for  
646 likelihood standard deviations increased with increasing noise, with repeated-measures ANOVA  
647 yielding a main factor of noise level ( $F(2) = 16.72$ ,  $p = 0.0003$ ) (Figure 5h). Post-hoc  
648 comparisons (Tukey HSD) showed that the standard deviation in the low noise condition (mean  
649 = 2.12, SE = 0.62) was significantly lower than in the medium (mean = 3.01, SE = 0.77;  $p =$   
650 0.0062) and high noise (mean = 3.53, SE = 0.83;  $p = 3.71 \times 10^{-5}$ ) conditions.

651 Finally, we assessed the correlation between slopes of lines fit to *model-generated*  
652 responses (i.e., using model-fit means and SDs) and *participants'* responses (Figure 5i). The  
653 correlation was strong and highly significant ( $r = 0.97$ ,  $p = 1.48 \times 10^{-20}$ ), suggesting that the fit  
654 parameters explained the data on a participant-by-participant basis. Overall, the results in  
655 Experiment 3 showed that participants' responses systematically moved closer to the prior with  
656 increasing sensory noise (Figure 5e-f) and that a Bayesian ideal-observer model largely  
657 explained the results (Figure 5g-i).

658

659 **Anti-Bayesian categorization is driven by image noise but not motor-driven noise**  
660 The above results showed that continuous perception across saccades is Bayesian, but  
661 categorical perception is anti-Bayesian. What gives rise to this puzzling dichotomy? Since  
662 behavior in other categorical tasks often *is* Bayesian (Wald, 1945; Ratcliff, 1978; Roitman and  
663 Shadlen, 2002; Bitzer et al., 2014; Hanks et al., 2014), our findings are likely more related to the  
664 perceptual system we studied than the task structure. In the visual system, object location is  
665 signaled via the organization of spatial receptive fields. Receptive fields are continuous from the  
666 retina to higher order visual areas (Colby et al., 1988; Engel et al., 1997; Golomb and  
667 Kanwisher, 2012a; Acaro and Livingstone, 2017) and maintain their retinotopic properties even

668 across eye movements (Golomb and Kanwisher, 2012b; Zimmerman et al., 2013) and when  
669 remapped (Hall and Colby, 2011; Neupane et al., 2020; Golomb and Mazer, 2021). Moreover,  
670 neurons in the frontal eye field use continuous tuning to represent object displacements across  
671 saccades (Crapse and Sommer, 2012), the stimulus quantity we probed directly. Thus, the  
672 intrinsic organization for processing visual location across saccades is in *continuous*  
673 coordinates. If reports of displacement are required in similarly continuous coordinates, the  
674 visual system is perhaps well-equipped to use a Bayes optimal strategy. Requiring a *categorical*  
675 report of the continuous system might necessitate an alternative strategy. This explanation has  
676 two important implications.

677 First, it implies that anti-Bayesian prior use was driven primarily by the organization of  
678 the *visual* system. A potential counterargument is that the Gaussian blob in Experiments 2 and  
679 3 was both the visual object and the saccade target. Blurring it might have added noise to the  
680 saccade and consequently the motor prediction (Figure 1a, black arrow), which depends on a  
681 copy of the saccade command, in addition to adding noise to the visual input (Figure 1a, red  
682 arrow). We did not find evidence of this, however. As a function of Gaussian blur, the standard  
683 deviations of saccadic endpoints (van Opstal and van Gisbergen, 1989; van Beers, 2007) did  
684 not change either parallel or perpendicular to the saccade in either the categorical (Experiment  
685 2; Figure 6a,b) or the continuous (Experiment 3; Figure 6c,d) experiment for humans  
686 (Repeated-measures ANOVAs:  $F(2) = 0.32$ ,  $p = 0.7306$  in Experiment 2 and  $F(3) = 1.55$ ,  $p =$   
687 0.2230 in Experiment 3 for endpoints parallel to the saccade;  $F(2) = 0.14$ ,  $p = 0.8693$  in  
688 Experiment 2 and  $F(3) = 2.6$ ,  $p = 0.1129$  in Experiment 3 for endpoints perpendicular to the  
689 saccade). Therefore, uncertainty in the visual input seems to have been the sole factor driving  
690 the anti-Bayesian prior use.

691 Second, the explanation that Bayesian prior use occurs in *continuous* report tasks for the  
692 *continuously-organized* visual system implies the converse: Bayesian prior use should occur in

693 categorical report tasks for systems having *categorical* properties. Making a saccade is one  
694 example. Each saccade poses an inherent, largely categorical sensory uncertainty in the form of  
695 saccadic suppression (Zuber and Stark, 1966; Bridgeman et al., 1975; Diamond et al., 2000;  
696 Reppas et al., 2002; Thiele et al., 2002; Bremmer et al., 2009, Wurtz, 2018). Visual processing  
697 is suppressed when a saccade is made, and not otherwise. This predicts that prior use would be  
698 Bayesian to compensate for saccadic suppression.

699 These considerations suggest a hypothesis that categorical tasks elicit (1) *anti-Bayesian*  
700 prior use if the sensory uncertainty is continuous (here, because it is represented in the  
701 continuously organized visual system), but (2) *Bayesian* prior use if the sensory uncertainty is  
702 categorical (here, because it is due to a saccade being made or not). In Experiments 4 and 5,  
703 respectively, we tested these hypotheses. We controlled for motor prediction uncertainty  
704 covarying with visual uncertainty by separating the blurred visual stimulus from the saccade  
705 target. The experiments used monkeys to permit precise eye position measurements with  
706 implanted scleral search coils (Robinson, 1963; Judge et al., 1980).

707 In Experiment 4 (Figure 6e), we selectively manipulated visual uncertainty by varying  
708 only the width of the Gaussian blob (i.e., the image noise), while the saccade target remained  
709 constant (Figure 6e, middle panel). The structure of Experiment 4 (Figure 6e, right panel) was  
710 nearly identical to Experiment 2 in humans: there were three noise levels (low, medium, and  
711 high). Low-noise, prior-training trials comprised 70% of all trials, while medium- and high-noise  
712 hypothesis-testing trials with neutral jump probability of 0.5 comprised 30% of trials. All trial  
713 types were randomly interleaved.

714 In Experiment 5 (Figure 6f), there were two levels of motor-driven uncertainty. In the  
715 “high uncertainty” condition, monkeys made a saccade to a target (to induce saccadic  
716 suppression) and reported whether a probe moved or not. In the “low uncertainty” condition,  
717 they withheld the saccade (no saccadic suppression) while the probe moved (Figure 6f, middle

718 panel). With- and no-saccade trials at three prior levels each were randomly interleaved (Figure  
 719 6f, right panel).

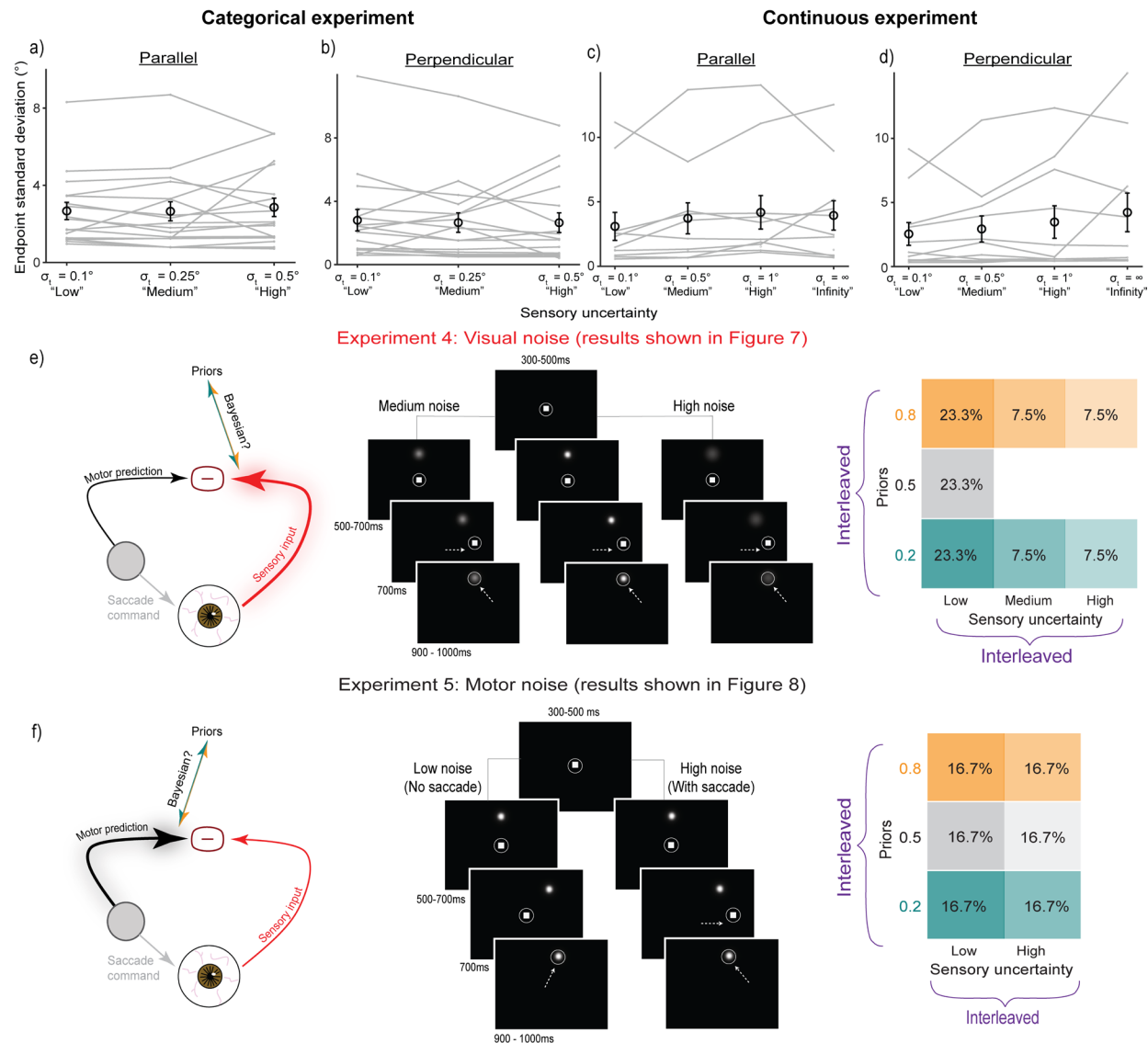


**Figure 6.** Image noise vs. motor-driven noise. a-d) Saccade endpoint scatter across the three image noise levels in Experiments 2 (Categorical) and 3 (Continuous), as quantified in the directions (a and c) perpendicular and (b and d) parallel to the saccade. (e-f) In monkeys, we separately tested how prior use changes with (e) image noise in Experiment 4 and (f) motor-driven noise in Experiment 5; for each experiment, the rationale (*left*), task events and stimulus configurations (*middle*), and trial breakdown (*right*) are schematized.

720 Results from Experiment 4 replicated the results from Experiment 2: the behavior was  
 721 anti-Bayesian (Figure 7). As expected from separating the visual probe from the saccade target,  
 722 there were no significant changes in standard deviations of saccade endpoints across noise

723 levels. The standard deviations [95% Confidence Intervals] for Monkey S were 1.01 [0.98, 1.06],  
724 0.97 [0.94, 1.03], and 0.96 [0.93, 1.00] for the low, medium, and high noise conditions. For  
725 Monkey T, they were 0.92 [0.86, 1.07], 0.84 [0.76, 1.00], and 0.93 [0.80, 1.19]. Hence prior use  
726 was driven by visual uncertainty with no detectable contribution of motor prediction uncertainty.

727 Both animals learned the priors as expected ( $P(J) = 0.2, 0.5$ , or  $0.8$ ), leading to an  
728 upward shift in psychometric functions for the high ( $P(J) = 0.8$ ) prior and a downward shift for the  
729 low ( $P(J) = 0.2$ ) prior (Figure 7a,b). Quantitatively, intercepts increased with increasing priors:  
730 0.08 [0.07, 0.10], 0.36 [0.33, 0.39] and 0.57 [0.53, 0.60] for Monkey S (Figure 7c, circles) and  
731 0.18 [0.15, 0.22], 0.33 [0.30, 0.36] and 0.40 [0.31, 0.45] for Monkey T (Figure 7c, triangles).

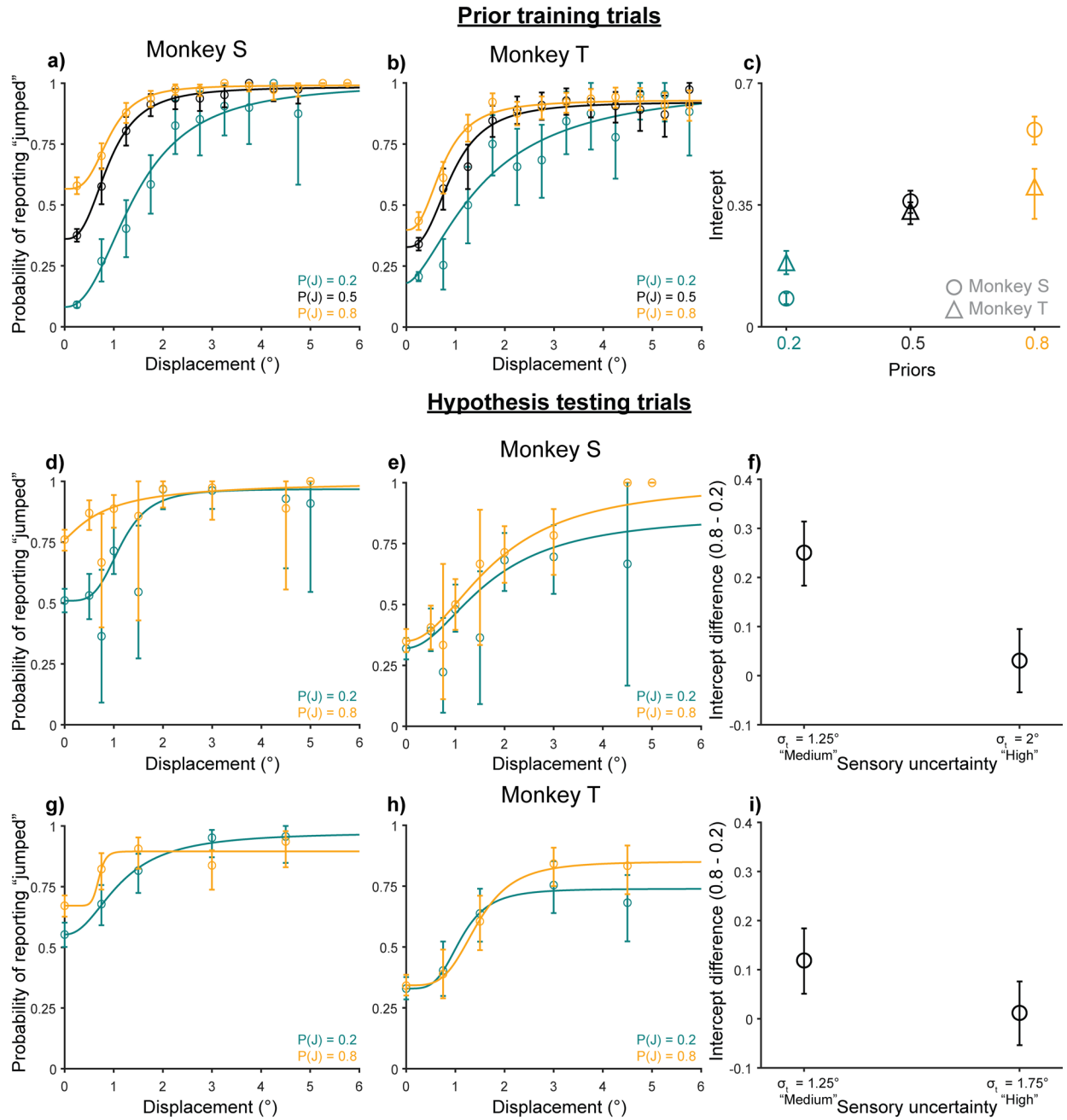


**Figure 7.** Experiment 4 results: Monkeys were anti-Bayesian for image noise. Monkey S: 10130 trials from 9 sessions. Monkey T: 9958 trials from 18 sessions. 95% confidence intervals bootstrapped from 10000 samples. a-c) Both animals' performance in prior learning trials in terms of psychometric curves (a: Monkey S; b: Monkey T) and intercept differences (c: both monkeys) matched the predictions of the Bayesian ideal observer model in Figure 3d,e. d-i) Prior use for both monkeys (d-f: Monkey S; g-i: Monkey T) was anti-Bayesian. They showed greater prior use in the medium noise condition (d and g) than in the high noise condition (e and h), as quantified by the intercept differences (f and i).

732           Also consistent with human participants, prior use *decreased* with increasing noise  
733           (Figure 7d-i). Psychometric functions for the 0.2 and 0.8 prior conditions got closer to each other  
734           with increasing noise for both Monkey S (Figure 7d,e) and Monkey T (Figure 7g,h), in contrast  
735           to the greater separation with noise predicted by a Bayesian model (Figure 4a,b). Intercept  
736           differences between the high- and low-prior conditions reflected this collapsing of curves.  
737           Monkey S had an intercept difference of 0.25 [0.18, 0.32] in the medium noise condition and  
738           0.03 [-0.03, 0.09] in the high noise condition. For Monkey T, it was 0.12 [0.05, 0.19] for medium  
739           noise and 0.01 [-0.05, 0.08] for high noise. Overall, the results showed that both monkeys used  
740           their priors less with increasing image noise. Note that the control experiment presented in  
741           Figure 4g-i also selectively varied the width of the Gaussian blob but not the saccade target,  
742           replicating the finding that prior use with increasing external, image uncertainty was anti-  
743           Bayesian regardless of task structure.

744           Experiment 5 showed, in contrast, that prior use to account for motor-related noise in the  
745           categorical task *was* Bayesian (Figure 8). Since early visual processing and sensitivity to  
746           displacements are suppressed around the time of saccades, we simulated motor-driven noise  
747           by increasing the standard deviation of the non-jump likelihood distribution in the with-saccade  
748           condition relative to the no-saccade condition ( $\sigma_{NJ} = 1^\circ$  and  $0.25^\circ$ , respectively) while holding the  
749           standard deviation of the jump likelihood distribution constant ( $\sigma_J = 5^\circ$ ). That is, larger  
750           displacements are perceived as “non-jumps” in the with-saccade condition to mimic the  
751           saccadic suppression of displacement.

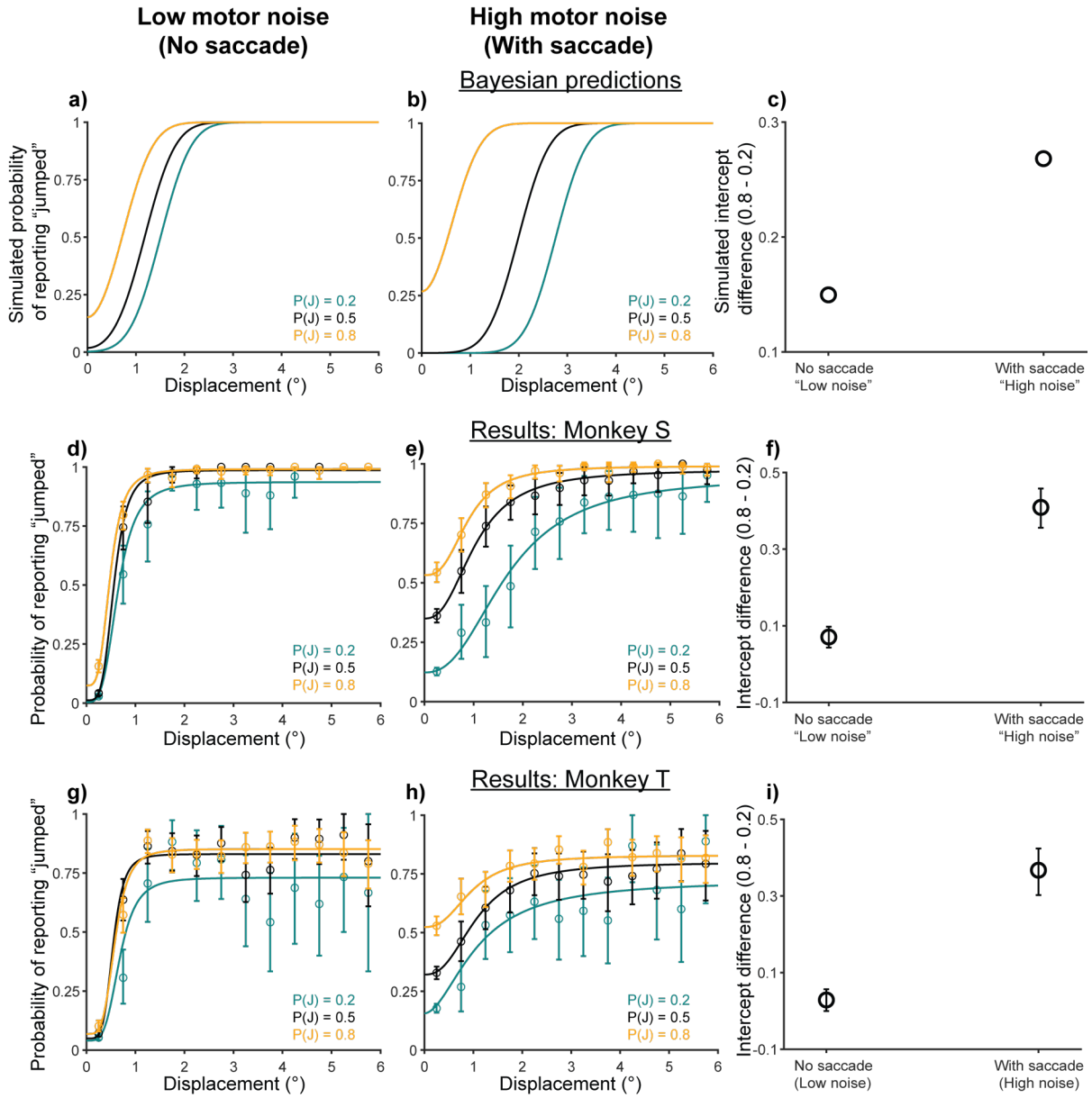


**Figure 8.** Experiment 5 results: Monkeys were Bayesian for motor-related noise. *Top row (a-c):* Predictions of the Bayesian ideal observer model for two levels of motor-driven noise. *Middle row (d-f):* Results from Monkey S. *Lower row (g-i):* Results from Monkey T. Unlike for image noise (Figure 7 and Figure 4h-i), the monkeys were decisively Bayesian in their use of priors to compensate for sensory uncertainty introduced by making a saccade.

752           The Bayesian model predicts that psychometric functions in the 0.2 and 0.8 prior  
 753           conditions would separate further (Figure 8a,b) and that the difference in intercepts between  
 754           them would be greater (Figure 8c) with greater motor-driven noise. Results from both monkeys  
 755           matched these model predictions. Psychometric curves for the different priors showed greater

756 separation when animals made a saccade (Figure 8e: Monkey S; Figure 8h: Monkey T; n =  
757 6000 analyzed trials for both animals) than in the condition without a saccade (Figure 8d:  
758 Monkey S; Figure 8g: Monkey T). The intercept difference between priors was 0.07 [0.04, 0.10]  
759 in the no-saccade condition and 0.41 [0.36, 0.46] when a saccade was made for Monkey S  
760 (Figure 8f), and 0.03 [-0.0007, 0.06] and 0.37 [0.30, 0.42] respectively for Monkey T (Figure 8i).

761 **A discriminative model provides a candidate explanation for anti-Bayesian categorization**

762 In sum, categorical judgments were Bayesian for motor-driven noise but anti-Bayesian for  
763 image noise. This leads to the question of how the anti-Bayesian behavior is generated. To  
764 address this, we sought to explain two aspects of the results across humans and monkeys that  
765 violated Bayesian predictions. First, prior use decreased with increasing image noise. Second,  
766 for human participants, the low prior (teal) curve rose above the baseline (black) curve in Figure  
767 3f, violating the Bayesian prediction of parallel prior psychometric curves (Figure 3d). Although  
768 prior curves were parallel for monkeys (Figure 7a,b and Figure 8e,h), this was after extensive  
769 training. Humans performed only single sessions. The early prior-training data from both  
770 monkeys were consistent with the human data (Figure 9a,b, teal curves rose above black  
771 curves). Therefore, an alternative model would have to explain the disproportionately high  
772 “jump” response rate for low priors early in training in addition to the decrease in prior use with  
773 increasing visual uncertainty.

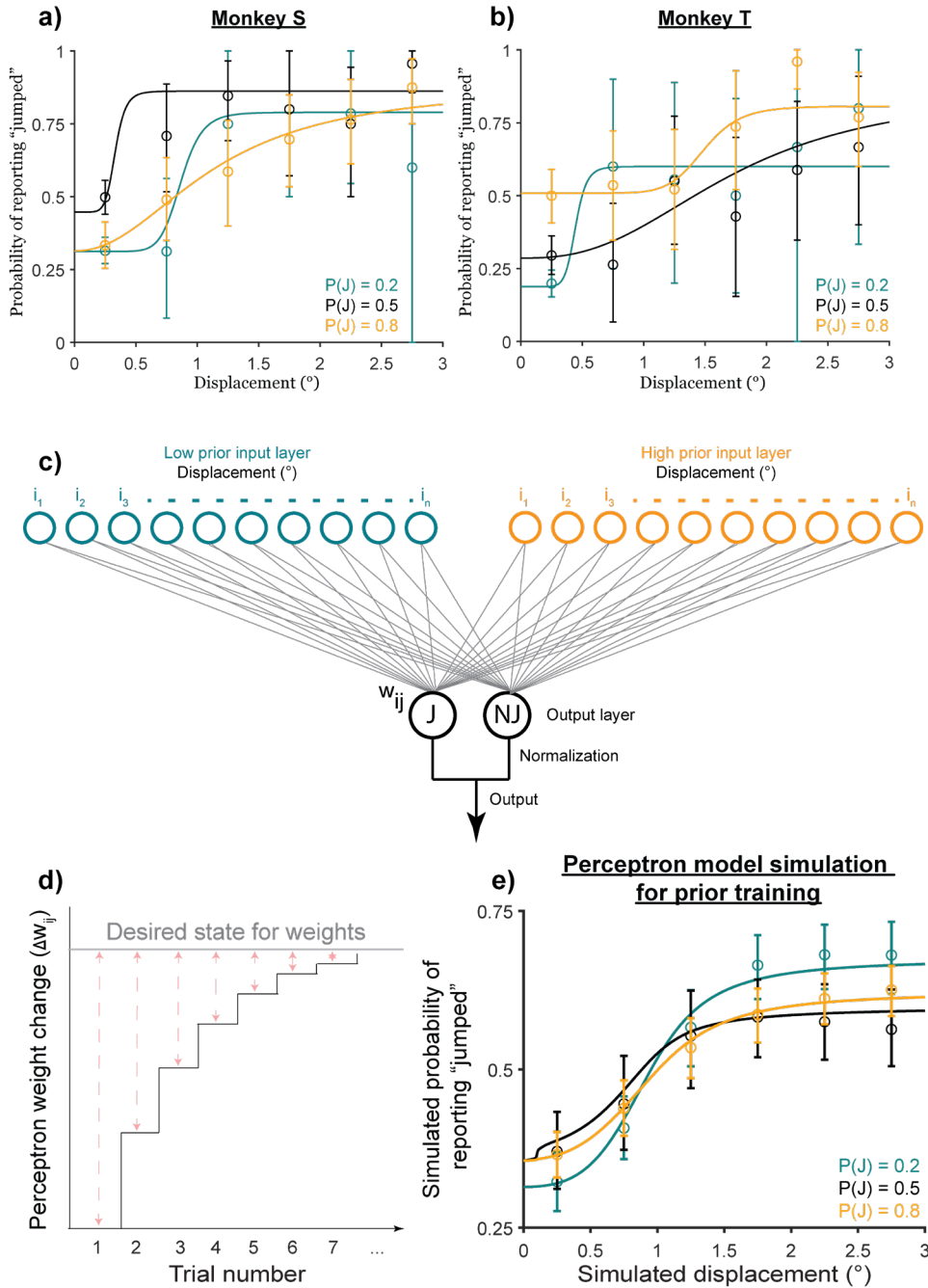


**Figure 9.** Discriminative (Perceptron) learning model. a-b) Early training results (Monkey S trials 1-500 and Monkey T trials 1-350 for each prior). c) Schematic of the discriminative model. d) Change in weights with each trial. e) Simulations of prior learning under the same conditions as the prior training trials in Experiment 2 on humans. Bins: averaged across 10000 simulations. Error bars: 95% CI. Psychometric curves are averaged across the simulations (blips at small displacements are an artifact of averaging across different inflection points).

774

An alternative framework to Bayesian models is discriminative models (Rumelhart et al.,

775

1986; Hinton, 1992; Ng and Jordan, 2002; Murphy, 2013), which directly learn to classify stimuli.

776 For our categorical task, a discriminative model would seek to classify continuous  
777 displacements into two categories, “jump” and “no jump.” We set up a simple two-layer neural  
778 network to classify displacements (Figure 9c) and simulated its performance under experimental  
779 conditions.

780 *Model structure*

781 The input layer consisted of units representing continuous displacements and the output layer  
782 had two units: “jump (J)” and “no jump (NJ).” For ease of computation, continuous input  
783 displacements were discretized into bins of  $0.1^\circ$ . Displacements ranged from  $0-7.5^\circ$ . That is,  
784 there were 75 input units for each network. Sensory noise was simulated as a Gaussian  
785 distribution of input unit activation, truncated at the two ends of the input range (0 and 7.5), such  
786 that the total activation of input units was always 1. On each trial, the distribution was centered  
787 on the true displacement for the trial and the width of activation was determined by the sensory  
788 noise level. Each input unit was connected to both output units. The activation of each output  
789 unit was the *weighted* sum of inputs, i.e.,

$$790 \quad a_j = \sum_{i=1}^n a_i w_{ij} \quad (25)$$

791 where  $a_j$  is the activation of the output unit, j;  $a_i$  is the activation of the output unit, i; and  $w_{ij}$  is  
792 the weight of the connection between input unit, i, and output unit, j. The final output on each  
793 trial was the normalized activation of the “jump” and “no jump” output units such that the output  
794 for each unit was bounded between 0 and 1:

$$795 \quad o_{jump} = \frac{a_{jump}}{a_{jump} + a_{no\ jump}} \quad (26)$$

796 and

797

$$o_{no\ jump} = \frac{a_{no\ jump}}{a_{jump} + a_{no\ jump}} \quad (27)$$

798 where  $o_{jump}$  is the final output of the “jump” unit,  $o_{no\ jump}$  is the final output of “no jump” unit,  
 799 and  $a_{jump}$  and  $a_{no\ jump}$  are activations of the “jump” and “no jump” output units, respectively.

800       The “knowledge” of the two categories is stored in the weights between the input and  
 801 output units, and the learned, category boundary takes the form of a psychometric function  
 802 reporting the probability that the target “jumped” given an input displacement. In other words,  
 803 the shape of the psychometric function is determined by the activation of the inputs and the  
 804 weights between inputs and outputs. Since psychometric curves have different shapes across  
 805 priors at the same point in training (e.g., Figure 3f), we assumed that the connections between  
 806 inputs and outputs (and their corresponding weights) are *prior-dependent*. This is equivalent to  
 807 the idea that distributions are learned separately across cue color contexts. We simulated the  
 808 prior-dependence of the input-output relationship by simply setting up separate sets of inputs for  
 809 each prior (low- and high-prior inputs illustrated in Figure 9c; simulations also included a  
 810 baseline  $P(J) = 0.5$  condition).

811       We next considered how the weights between inputs and outputs might be updated. One  
 812 possibility was that they are updated by a simple Hebbian-like associative learning rule (Hebb,  
 813 1949) where weights between two units are updated in a manner proportional to their activation.  
 814 We chose a slight variation of this rule based on work by Gluck and Bower (1988), who showed  
 815 that an *error-based* learning rule, rather than a purely associative learning rule, leads to a  
 816 disproportionate overweighting of infrequent events early in training.

817       The learning rule is given by:

818

$$\Delta w_{ij} = \beta a_i(d - o_j) \quad (28)$$

819 where  $\Delta w_{ij}$  is the change in weights between input unit, i, and output unit, j;  $\beta$  is the learning  
820 rate,  $a_i$  is the activation of the input unit, i;  $o_j$  is the final output of unit j, and d is the desired  
821 state of output unit, j. The term  $(d - o_j)$  is therefore the error between the current output of the  
822 model and the desired state determined by feedback on each trial. In summary, the change in  
823 weights or learning on each trial is proportional to the activity of the input and the error of the  
824 model on that trial. This is equivalent to the Perceptron learning rule (Rosenblatt, 1957; Minsky  
825 and Papert, 1969). For infrequent events such as large displacements in the low prior condition,  
826 the weight changes between the event and the output early in training are relatively large (left  
827 side of Figure 9d). Taking a snapshot of performance at this stage would thus result in an  
828 apparent overweighting of their contribution to the output as seen early in training in Figures 3f,  
829 9a, and 9b. This rule, however, predicts that once weights asymptote towards the desired state  
830 late in training (right side of Figure 9d), events should contribute to the model's performance in a  
831 manner proportional to their relative frequencies, and psychometric curves should become  
832 parallel to one another as seen in Figures 7a, 7b, 8e, and 8h.

833 *Simulations*

834 We evaluated the model's ability to explain the results by simulating its performance under  
835 experimental conditions. 95% confidence intervals for each simulated estimate were obtained  
836 by running 10000 simulations and identifying the middle 95% of each estimate, i.e., 2.5  
837 percentile – 97.5 percentile. We simulated early prior training by following the same  
838 experimental structure as for the human experiments: a baseline block at  $P(J) = 0.5$  followed by  
839 two 600-trial blocks at  $P(J) = 0.8$  and  $P(J) = 0.2$ , respectively. Of those trials, 70% were prior  
840 training trials at the lowest noise level,  $\sigma_{\text{target}} = 0.1^\circ$ . The remaining 30% were medium ( $\sigma_{\text{target}} =$   
841  $1^\circ$ ) and high-noise ( $\sigma_{\text{target}} = 2^\circ$ ) testing trials with a neutral movement statistic of 0.5 but  
842 simulated using the same inputs as the prior condition. Displacements were drawn from  
843 overlapping Gaussian distributions as in the experiments. Jumps were drawn from a distribution

844 with  $\mu_{\text{jump}} = 0^\circ$ ,  $\sigma_{\text{jump}} = 2.5^\circ$ , and non-jumps were drawn from a distribution with  $\mu_{\text{non-jump}} = 0^\circ$ ,  $\sigma_{\text{non-}}$   
845  $\text{jump} = 0.5^\circ$ . On trials where the target jumped, the desired state was set to 1 for the “jump” output  
846 unit and 0 for the “no jump” output unit. On trials where the target did not jump, it was set to 0  
847 for the “jump” unit and 1 for the “no jump” unit. The learning rate was set at 0.5. As expected,  
848 the outputs recapitulated the disproportionately high response rate for large displacements in  
849 the low prior condition (Figure 9e, teal curve). However, it also downweighted the infrequent  
850 small displacements in the high prior condition (Figure 9e, orange curve). To account for this,  
851 we considered that reports in the categorical task may result from a *combination* of a  
852 discriminative and a Bayesian model. The Bayesian prior use for high saccade-driven  
853 uncertainty raises high prior intercepts (Figure 8e,h) and thus could compensate for the  
854 downweighting by the discriminative model.

855 Therefore, we next simulated a combined model whose final output was a weighted  
856 combination of outputs from the discriminative model, which incorporated visual noise, and a  
857 Bayesian ideal observer model which incorporated motor-driven noise (Figure 10a). Motor noise  
858 was simulated only in the Bayesian model by setting the width of the non-jump distribution,  $\sigma_{\text{non-}}$   
859  $\text{jump} = 1.5^\circ$ , i.e., triple the width of the simulated experimental distribution to mimic saccadic  
860 suppression. Bayesian and discriminative model outputs were combined linearly, such that:

$$861 \quad O_C = w_B O_B + w_P O_P \quad (29)$$

862 where  $O_C$  is the output of the combined model,  $O_B$  is the output of the Bayesian model,  $O_P$  is the  
863 output of the discriminative model, and  $w_B$  and  $w_P$  are the weights assigned to the Bayesian  
864 and discriminative model, respectively. Further, the weights of the two component models  
865 added up to 1:

$$866 \quad w_b + w_P = 1 \quad (30)$$

867 We combined the outputs of the Bayesian and discriminative models at relative weights of 0.1  
 868 and 0.9, respectively, to generate the data in Figure 10b, where the pattern of the curves  
 869 matched data from human participants well.

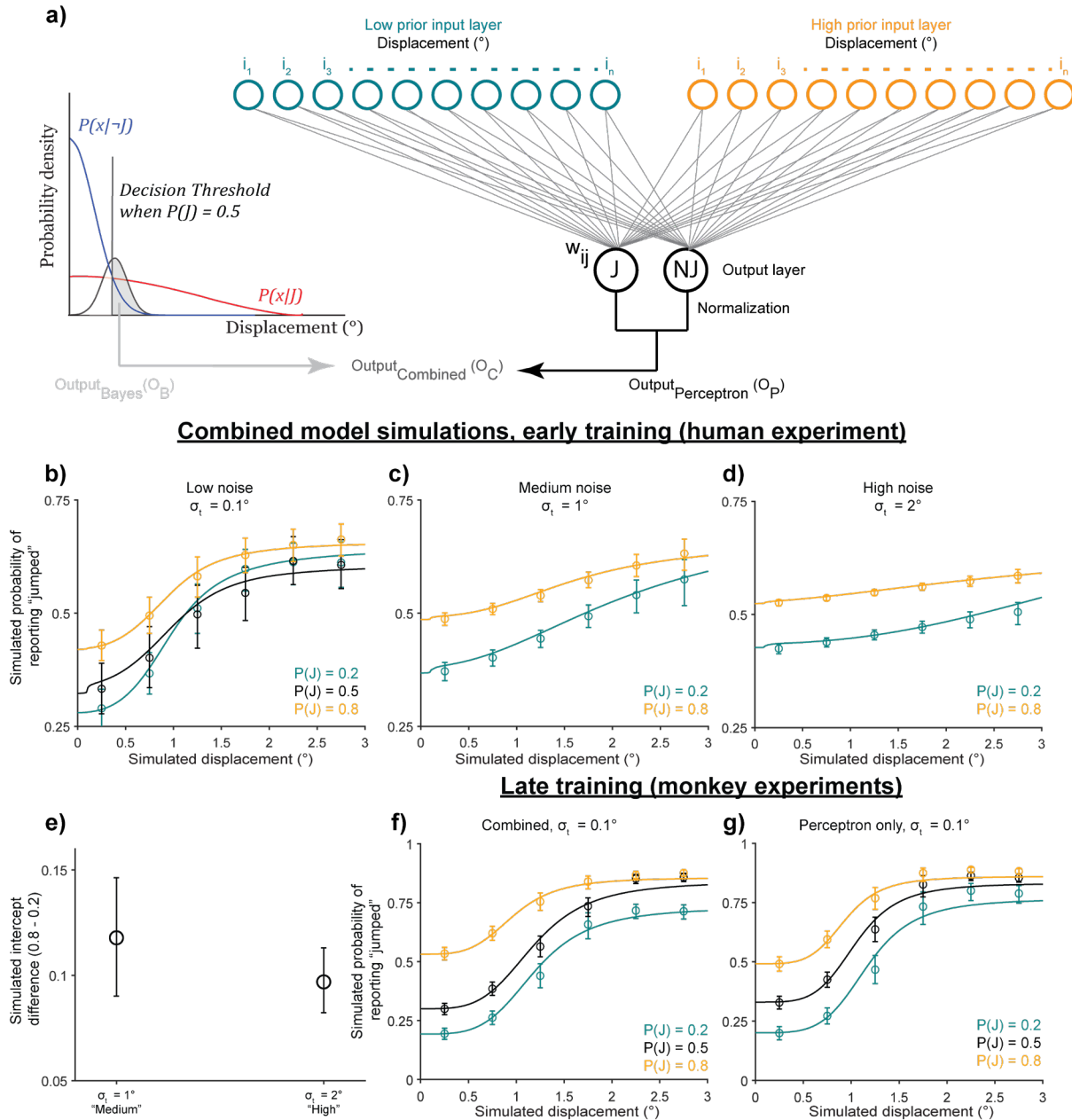


**Figure 10.** Combined Bayesian and discriminative model. a) Schematic of the Bayesian model output (from Figure 3a) on the left being combined with the output from the discriminative (Perceptron) model. b-d) Psychometric curves simulated under the same experimental conditions as the human experiment for (b) low, (c) medium, and (d) high noise levels. Bins: averaged across 10000 simulations. Error bars: 95% CI. Psychometric curves are averaged across the simulations (blips at small displacements are an artifact of averaging across different

inflection points). e) Intercept differences across the medium and high noise conditions. f-g) Late training data for (f) the combined model and (g) the discriminative model alone.

870 Next, adding medium and high noise to the visual input of the discriminative model (but  
871 holding visual noise constant in the Bayesian model) caused psychometric curves to move  
872 closer to each other with increasing noise (Figure 10c,d), as quantified by the downward trend in  
873 high-low prior intercept differences (Figure 10e). Finally, we tested the prediction that prior  
874 curves become parallel once weights approach a relatively stable desired state for all input units  
875 (Figure 9d, right side) by letting the model run for 5000 trials. Data from trials 3000-5000 for the  
876 combined (discriminative + Bayesian) model (Figure 10f) and for the discriminative model alone  
877 (Figure 10g) support this prediction.

878 In summary, the combined model recapitulated both the surprising trade-off between  
879 priors and noise and the long-term learning effects that were unexplained by a Bayesian ideal  
880 observer model alone. This demonstrated that a discriminative learning rule provides a feasible  
881 explanation for the anti-Bayesian results, and that the categorization of object displacement  
882 across saccades is governed by both Bayesian and discriminative processes.

883

## 884 DISCUSSION

885 We found that human participants were Bayesian for continuous reports of object displacement  
886 across saccades but anti-Bayesian for categorical reports. Further investigation in monkeys  
887 showed that the anti-Bayesian effect was primarily due to external, image noise rather than  
888 motor-driven noise. The use of a Perceptron-like, discriminative learning rule provides a  
889 candidate explanation for anti-Bayesian performance in the categorization task.

890 Limitations of the experimental design and modeling choices should be considered while  
891 interpreting the results. First, it is possible that the anti-Bayesian result is a consequence of how  
892 we conceptualized parameters (e.g., the prior, or sensory noise) in the categorical Bayesian

ideal observer model. For example, for continuous tasks, it has been shown that if the sensory likelihood is asymmetric in a way that can result from assumptions of efficient sensory encoding, then the outcome of a Bayesian decoding process can be seemingly anti-Bayesian (Wei and Stocker, 2015). Of course, alternative parameters might predict the surprising results. However, we chose simulation parameters to closely map onto experimental parameters and mimic empirical phenomena such as saccadic suppression. As a result, the model captures both the Bayesian trade-off with motor-driven noise and the anti-Bayesian trade-off with visual noise. To our best estimate, there was no simple set of alternative parameters that did so parsimoniously.

Second, we limited the simulation of motor-induced noise in Experiment 5 to just one phenomenon, i.e., saccadic suppression. We did this by increasing the width of the non-jump likelihood,  $P(x|\neg J)$ . We focused on saccadic suppression since it is largely a categorical form of uncertainty that is present when a saccade is made, and not otherwise. It was thus sufficient for testing our hypothesis. However, there are other ways in which saccades influence vision both at the level of behavior and neurons. Such effects include compression of space toward the saccade target (Honda, 1993; Awader and Lappe, 2006; Hamker et al., 2011; Pola, 2011) or the shifting or smearing of visual receptive fields around the time of saccades (Neupane et al., 2020; Golomb and Mazer, 2021). Indeed, the magnitude of saccadic suppression may vary with saccade amplitude (Stevenson et al., 1986) and the direction in which the probe moves relative to the saccade vector (Niemeier et al., 2003; Crapse and Sommer, 2012). Our results do not preclude the inclusion of additional, fine-grained motor-induced phenomena into the normative model, and the resulting predictions would be testable. Another consideration for Experiment 5 is that in the no-saccade condition of the task, animals fixated a central square for the duration of a trial. We did not prevent the animal from making fixational eye movements such as microsaccades (Martinez-Conde et al., 2004), and saccadic suppression may occur around the time of microsaccades (Bair and O'Keefe, 1998; Hafed and Krauzlis, 2010; Martinez-Conde et al., 2013; Hafed et al., 2015). Although we did not control for microsaccades, the stimulus

919 displacement was not timed to microsaccade onset in no-saccade trials as it was to saccade  
920 onset in with-saccade trials. On average, therefore, the influence of (micro)saccadic  
921 suppression should be quite low in the no-saccade condition.

922 Finally, we limited the scope of the discriminative and combined models to provide a  
923 candidate alternative to the *categorical* Bayesian model with minimal additional assumptions.  
924 This leaves some unexplained patterns in the data, e.g., overall intercepts across priors  
925 decrease with increasing noise for humans (Figure 4d,e) and monkeys (Figure 7d,e,g,h) but not  
926 for the model (Figure 10b-d). Similarly, for our experimental-like parameters, the model does not  
927 capture the complete collapse of prior curves with increasing noise. The model may be  
928 extended, however, to include additional components such as Bayesian integration in the  
929 *continuous* input layer (from Experiment 3) to better explain the data. Assumptions about how  
930 the components combine may additionally be testable too.

931 The overall pattern of results in our study poses a fundamental question: what  
932 determines the use of Bayesian vs. discriminative models for perception? Despite recent efforts  
933 to acknowledge the contribution of both Bayesian and non-Bayesian models to perception  
934 (Liquitaine and Gardner, 2018; Rahnev and Denison, 2018; Gardner, 2019; Sohn and Jazayeri,  
935 2021; DiCarlo et al., 2021), the field lacks a synthesized, theoretical account of when Bayesian  
936 models are used and when they are not. As we noted while motivating Experiments 4 and 5, our  
937 results suggest a link between the inherent neural organization of sensorimotor systems and  
938 Bayesian behavior. Further clarification of this link would allow our understanding of each to  
939 constrain and advance our understanding of the other.

940 Although our study was specific to visual-oculomotor behavior, we expect that the  
941 conclusions extend to other sensorimotor systems. Accounting for self-movement is an issue for  
942 almost all sensory modalities, and the integration of movement and sensory signals for active  
943 perception has been observed widely in the brain (Niell and Stryker, 2010; Keller et al., 2012;  
944 Schneider and Mooney, 2018; Crapse and Sommer, 2008). Understanding the relative

945 contributions of Bayesian and discriminative computations to active vision may guide future  
946 studies on how expectations, self-movement, and external sensory information combine for  
947 more general forms of active perception.

948

949 **REFERENCES**

950 Arcaro, M. J., & Livingstone, M. S. (2017). A hierarchical, retinotopic proto-organization of the  
951 primate visual system at birth. *ELife*, 6, e26196.

952 Awater, H., & Lappe, M. (2006). Mislocalization of Perceived Saccade Target Position Induced  
953 by Perisaccadic Visual Stimulation. *Journal of Neuroscience*, 26(1), 12–20.  
954 <https://doi.org/10.1523/JNEUROSCI.2407-05.2006>

955 Bair, W., & O'Keefe, L. P. (1998). The influence of fixational eye movements on the response of  
956 neurons in area MT of the macaque. *Visual Neuroscience*, 15(4), 779–786.  
957 <https://doi.org/10.1017/S0952523898154160>

958 Bajcsy, R. (1988). Active perception. *Proceedings of the IEEE*, 76(8), 966–1005.  
959 <https://doi.org/10.1109/5.5968>

960 Barlow, H. B. (1961). Possible principles underlying the transformation of sensory  
961 messages. *Sensory communication*, 1(01).

962 Bitzer, S., Park, H., Blankenburg, F., Kiebel, S. J. (2014) Perceptual decision making: Drift-  
963 diffusion model is equivalent to a Bayesian model. *Frontiers in Human Neuroscience*, 8:  
964 102. DOI: <https://doi.org/10.3389/fnhum.2014.00102>

965 Bremmer, F., Kubischik, M., Hoffmann, K.-P., & Krekelberg, B. (2009). Neural Dynamics of  
966 Saccadic Suppression. *Journal of Neuroscience*, 29(40), 12374–12383.  
967 <https://doi.org/10.1523/JNEUROSCI.2908-09.2009>

- 968 Bridgeman, B., Hendry, D., & Stark, L. (1975). Failure to detect displacement of the visual world  
969 during saccadic eye movements. *Vision Research*, 15(6), 719–722.  
970 [https://doi.org/10.1016/0042-6989\(75\)90290-4](https://doi.org/10.1016/0042-6989(75)90290-4)
- 971 Britten, K. H., Newsome, W. T., Shadlen, M. N., Celebrini, S., & Movshon, J. A. (1996). A  
972 relationship between behavioral choice and the visual responses of neurons in macaque  
973 MT. *Visual Neuroscience*, 13(1), 87–100. <https://doi.org/10.1017/s095252380000715x>
- 974 Colby, C. L., Gattass, R., Olson, C. R., & Gross, C. G. (1988). Topographical organization of  
975 cortical afferents to extrastriate visual area PO in the macaque: A dual tracer study.  
976 *Journal of Comparative Neurology*, 269(3), 392–413.  
977 <https://doi.org/10.1002/cne.902690307>
- 978 Crapse, T. B. & Sommer, M. A. (2012). Frontal Eye Field Neurons Assess Visual Stability  
979 Across Saccades. *Journal of Neuroscience*. 32, 2835–2845
- 980 Crapse, T. B., & Sommer, M. A. (2008). Corollary discharge across the animal kingdom. *Nature  
981 Reviews Neuroscience*, 9(8), 587–600. <https://doi.org/10.1038/nrn2457>
- 982 Crevecoeur, F., & Kording, K. P. (2017). Saccadic suppression as a perceptual consequence of  
983 efficient sensorimotor estimation. *eLife*, 6, e25073. <https://doi.org/10.7554/eLife.25073>
- 984 Darlington, T. R., Tokiyama, S., & Lisberger, S. G. (2017). Control of the strength of visual-  
985 motor transmission as the mechanism of rapid adaptation of priors for Bayesian  
986 inference in smooth pursuit eye movements. *Journal of Neurophysiology*, 118(2), 1173–  
987 1189. <https://doi.org/10.1152/jn.00282.2017>
- 988 Diamond, M. R., Ross, J., & Morrone, M. C. (2000). Extraretinal control of saccadic  
989 suppression. *The Journal of Neuroscience: The Official Journal of the Society for  
990 Neuroscience*, 20(9), 3449–3455.

- 991 DiCarlo, J. J., Haefner, R., Isik, L., Konkle, T., Kriegeskorte, N., Peters, B., Rust, N.,
- 992 Stachenfeld, K., Tenenbaum, J. B., Tsao, D., & Yildirim, I. (2021). *How does the brain*  
993 *combine generative models and direct discriminative computations in high-level vision?*
- 994 <https://openreview.net/forum?id=zITiwFtLIR4>
- 995 Engel, S. A., Glover, G. H., & Wandell, B. A. (1997). Retinotopic organization in human visual  
996 cortex and the spatial precision of functional MRI. *Cerebral Cortex*, 7(2), 181–192.
- 997 Ernst, M. O., & Banks, M. S. (2002). Humans integrate visual and haptic information in a  
998 statistically optimal fashion. *Nature*, 415(6870), 429–433.
- 999 <https://doi.org/10.1038/415429a>
- 1000 Feinberg, I., & Guazzelli, M. (1999). Schizophrenia—A disorder of the corollary discharge  
1001 systems that integrate the motor systems of thought with the sensory systems of  
1002 consciousness. *The British Journal of Psychiatry: The Journal of Mental Science*, 174,  
1003 196–204. <https://doi.org/10.1192/bjp.174.3.196>
- 1004 Fetsch, C. R., Pouget, A., DeAngelis, G. C., & Angelaki, D. E. (2012). Neural correlates of  
1005 reliability-based cue weighting during multisensory integration. *Nature Neuroscience*,  
1006 15(1), 146–154. <https://doi.org/10.1038/nn.2983>
- 1007 Ford, J. M., & Mathalon, D. H. (2005). Corollary discharge dysfunction in schizophrenia: Can it  
1008 explain auditory hallucinations? *International Journal of Psychophysiology: Official*  
1009 *Journal of the International Organization of Psychophysiology*, 58(2–3), 179–189.
- 1010 <https://doi.org/10.1016/j.ijpsycho.2005.01.014>
- 1011 Gardner, J. L. (2019). Optimality and heuristics in perceptual neuroscience. *Nature*  
1012 *Neuroscience*, 22(4), 514–523. <https://doi.org/10.1038/s41593-019-0340-4>
- 1013 Gibson, J. J. (1966). *The senses considered as perceptual systems*. Houghton Mifflin.

- 1014 Girshick, A. R., Landy, M. S., & Simoncelli, E. P. (2011). Cardinal rules: Visual orientation  
1015 perception reflects knowledge of environmental statistics. *Nature Neuroscience*, 14(7),  
1016 926–932. <https://doi.org/10.1038/nn.2831>
- 1017 Gluck, M. A., & Bower, G. H. (1988). From conditioning to category learning: An adaptive  
1018 network model. *Journal of Experimental Psychology: General*, 117(3), 227–247.  
1019 <https://doi.org/10.1037/0096-3445.117.3.227>
- 1020 Golomb, J. D., & Kanwisher, N. (2012a). Higher level visual cortex represents retinotopic, not  
1021 spatiotopic, object location. *Cerebral Cortex*, 22(12), 2794–2810.
- 1022 Golomb, J. D., & Kanwisher, N. (2012b). Retinotopic memory is more precise than spatiotopic  
1023 memory. *Proceedings of the National Academy of Sciences*, 109(5), 1796–1801.
- 1024 Golomb, J. D., & Mazer, J. A. (2021). Visual Remapping. *Annual Review of Vision Science*, 7,  
1025 257–277. <https://doi.org/10.1146/annurev-vision-032321-100012>
- 1026 Green, D. M., & Swets, J. A. (1966). *Signal detection theory and psychophysics* (pp. xi, 455).  
1027 John Wiley.
- 1028 Hafed, Z. M., & Krauzlis, R. J. (2010). Microsaccadic Suppression of Visual Bursts in the  
1029 Primate Superior Colliculus. *Journal of Neuroscience*, 30(28), 9542–9547.  
1030 <https://doi.org/10.1523/JNEUROSCI.1137-10.2010>
- 1031 Hafed, Z. M., Chen, C.-Y., & Tian, X. (2015). Vision, Perception, and Attention through the Lens  
1032 of Microsaccades: Mechanisms and Implications. *Frontiers in Systems Neuroscience*, 9.  
1033 <https://www.frontiersin.org/article/10.3389/fnsys.2015.00167>
- 1034 Hall, N. J., & Colby, C. L. (2011). Remapping for visual stability. *Philosophical Transactions of  
1035 the Royal Society B: Biological Sciences*, 366(1564), 528–539.  
1036 <https://doi.org/10.1098/rstb.2010.0248>

- 1037 Hamker, F. H., Zirnsak, M., Ziesche, A., & Lappe, M. (2011). Computational models of spatial  
1038 updating in peri-saccadic perception. *Philosophical Transactions of the Royal Society of*  
1039 *London. Series B, Biological Sciences.* <https://doi.org/10.1098/rstb.2010.0229>
- 1040 Hanks, T., Kiani, R., & Shadlen, M. N. (2014). A neural mechanism of speed-accuracy tradeoff  
1041 in macaque area LIP. *eLife*, 3, e02260. <https://doi.org/10.7554/eLife.02260>
- 1042 Hebb, D. O. (1949). The organization of behavior; a neuropsychological theory(pp. xix, 335).  
1043 Wiley.
- 1044 Hinton, G. E. (1992). How neural networks learn from experience. *Scientific American*, 267(3),  
1045 144–151. <https://doi.org/10.1038/scientificamerican0992-144>
- 1046 Honda, H. (1993). Saccade-contingent displacement of the apparent position of visual stimuli  
1047 flashed on a dimly illuminated structured background. *Vision Research*, 33(5–6), 709–  
1048 716. [https://doi.org/10.1016/0042-6989\(93\)90190-8](https://doi.org/10.1016/0042-6989(93)90190-8)
- 1049 Jacobs, R. A. (1999). Optimal integration of texture and motion cues to depth. *Vision Research*,  
1050 39(21), 3621–3629. [https://doi.org/10.1016/s0042-6989\(99\)00088-7](https://doi.org/10.1016/s0042-6989(99)00088-7)
- 1051 Jazayeri, M., & Shadlen, M. N. (2010). Temporal context calibrates interval timing. *Nature*  
1052 *Neuroscience*, 13(8), 1020–1026. <https://doi.org/10.1038/nn.2590>
- 1053 Johnson, K. O. (2000). Neural Coding. *Neuron*, 26(3), 563–566. [https://doi.org/10.1016/S0896-6273\(00\)81193-9](https://doi.org/10.1016/S0896-<br/>1054 6273(00)81193-9)
- 1055 Judge, S. J., Richmond, B. J., & Chu, F. C. (1980). Implantation of magnetic search coils for  
1056 measurement of eye position: An improved method. *Vision Research*, 20(6), 535–538.  
1057 [https://doi.org/10.1016/0042-6989\(80\)90128-5](https://doi.org/10.1016/0042-6989(80)90128-5)

- 1058 Keller, G. B., Bonhoeffer, T., & Hübener, M. (2012). Sensorimotor Mismatch Signals in Primary  
1059 Visual Cortex of the Behaving Mouse. *Neuron*, 74(5), 809–815.
- 1060 <https://doi.org/10.1016/j.neuron.2012.03.040>
- 1061 Knill, D. C., & Richards, W. (1996). *Perception as Bayesian Inference*. Cambridge University  
1062 Press.
- 1063 Knill, D. C., & Saunders, J. A. (2003). Do humans optimally integrate stereo and texture  
1064 information for judgments of surface slant? *Vision Research*, 43(24), 2539–2558.
- 1065 [https://doi.org/10.1016/s0042-6989\(03\)00458-9](https://doi.org/10.1016/s0042-6989(03)00458-9)
- 1066 Kording, K. P., & Wolpert, D. M. (2004). Bayesian integration in sensorimotor learning. *Nature*,  
1067 427(6971), 244–247. <https://doi.org/10.1038/nature02169>
- 1068 Laquitaine, S., & Gardner, J. L. (2018). A Switching Observer for Human Perceptual Estimation.  
1069 *Neuron*, 97(2), 462-474.e6. <https://doi.org/10.1016/j.neuron.2017.12.011>
- 1070 Martinez-Conde, S., Macknik, S. L., & Hubel, D. H. (2004). The role of fixational eye movements  
1071 in visual perception. *Nature Reviews Neuroscience*, 5(3), 229–240.
- 1072 <https://doi.org/10.1038/nrn1348>
- 1073 Martinez-Conde, S., Otero-Millan, J., & Macknik, S. L. (2013). The impact of microsaccades on  
1074 vision: Towards a unified theory of saccadic function. *Nature Reviews Neuroscience*,  
1075 14(2), 83–96. <https://doi.org/10.1038/nrn3405>
- 1076 Matsuda, K., Nagami, T., Sugase, Y., Takemura, A., & Kawano, K. (2017). A Widely Applicable  
1077 Real-Time Mono/Binocular Eye Tracking System Using a High Frame-Rate Digital  
1078 Camera. In M. Kurosu (Ed.), *Human-Computer Interaction. User Interface Design,  
1079 Development and Multimodality* (pp. 593–608). Springer International Publishing.
- 1080 [https://doi.org/10.1007/978-3-319-58071-5\\_45](https://doi.org/10.1007/978-3-319-58071-5_45)

- 1081 Minsky, M., & Papert, S. A. (1969). Perceptrons: An Introduction to Computational Geometry.  
1082 MIT Press.
- 1083 Murphy, K. P. (2013). Machine learning: a probabilistic perspective. Cambridge, Mass. [u.a.]:  
1084 MIT Press.
- 1085 Neupane, S., Guitton, D., & Pack, C. C. (2020). Perisaccadic remapping: What? How? Why?  
1086 *Reviews in the Neurosciences*, 31(5), 505–520. <https://doi.org/10.1515/revneuro-2019-0097>
- 1088 Ng, A. Jordan, M.I. (2002) On discriminative vs. generative classifiers: A comparison of logistic  
1089 regression and naive bayes. *Advances in Neural Information Processing Systems* 14,  
1090 841
- 1091 Niell, C. M., & Stryker, M. P. (2010). Modulation of visual responses by behavioral state in  
1092 mouse visual cortex. *Neuron*, 65(4), 472–479.  
1093 <https://doi.org/10.1016/j.neuron.2010.01.033>
- 1094 Niemeier, M., Crawford, J. D., & Tweed, D. B. (2003). Optimal transsaccadic integration  
1095 explains distorted spatial perception. *Nature*, 422(6927), 76–80.  
1096 <https://doi.org/10.1038/nature01439>
- 1097 Parr, T., & Friston, K. J. (2017). The active construction of the visual world. *Neuropsychologia*,  
1098 104, 92–101. <https://doi.org/10.1016/j.neuropsychologia.2017.08.003>
- 1099 Pola, J. (2011). An explanation of perisaccadic compression of visual space. *Vision Research*,  
1100 51(4), 424–434. <https://doi.org/10.1016/j.visres.2010.12.010>
- 1101 Rahnev, D., & Denison, R. N. (2018). Suboptimality in perceptual decision making. *Behavioral  
1102 and Brain Sciences*, 41. <https://doi.org/10.1017/S0140525X18000936>

- 1103 Rao, H. M., Abzug, Z. M., & Sommer, M. A. (2016). Visual continuity across saccades is  
1104 influenced by expectations. *Journal of Vision*, 16(5), 7. <https://doi.org/10.1167/16.5.7>
- 1105 Rao, R. P. N., & Ballard, D. H. (1999). Predictive coding in the visual cortex: A functional  
1106 interpretation of some extra-classical receptive-field effects. *Nature Neuroscience*, 2(1),  
1107 79–87. <https://doi.org/10.1038/4580>
- 1108 Ratcliff, R. (1978) A theory of memory retrieval. *Psychological Review*, 85(2): 59–108.
- 1109 Reppas, J. B., Usrey, W. M., & Reid, R. C. (2002). Saccadic eye movements modulate visual  
1110 responses in the lateral geniculate nucleus. *Neuron*, 35(5), 961–974.  
1111 [https://doi.org/10.1016/s0896-6273\(02\)00823-1](https://doi.org/10.1016/s0896-6273(02)00823-1)
- 1112 Robinson, D. A. (1963). A Method of Measuring Eye Movement Using a Scleral Search Coil in a  
1113 Magnetic Field. *IEEE Transactions on Bio-Medical Electronics*, 10(4), 137–145.  
1114 <https://doi.org/10.1109/TBME.1963.4322822>
- 1115 Roitman, J. D., Shadlen, M. N. (2002) Response of neurons in the lateral intraparietal area  
1116 during a combined visual discrimination reaction time task. *Journal of Neuroscience*,  
1117 22(21): 9475–9489. DOI: <https://doi.org/10.1523/JNEUROSCI.22-21-09475.2002>
- 1118 Rosenblatt, Frank (1957). "The Perceptron—a perceiving and recognizing automaton". Report  
1119 85-460-1. Cornell Aeronautical Laboratory.
- 1120 Rumelhart, D. E., McClelland, J. L., & Group, P. R. (1986). *Parallel Distributed Processing:*  
1121 *Explorations in the Microstructure of Cognition: Foundations* (Vol. 1). A Bradford Book.
- 1122 Schneider, D. M., & Mooney, R. (2018). How Movement Modulates Hearing. *Annual Review of  
1123 Neuroscience*, 41, 553–572. <https://doi.org/10.1146/annurev-neuro-072116-031215>

- 1124 Sohn, H., & Jazayeri, M. (2021). Validating model-based Bayesian integration using prior–cost  
1125 metamers. *Proceedings of the National Academy of Sciences*, 118(25).
- 1126 <https://doi.org/10.1073/pnas.2021531118>
- 1127 Sommer, M. A., & Wurtz, R. H. (2002). A Pathway in Primate Brain for Internal Monitoring of  
1128 Movements. *Science*, 296(5572), 1480–1482. <https://doi.org/10.1126/science.1069590>
- 1129 Sommer, M. A., & Wurtz, R. H. (2006). Influence of the thalamus on spatial visual processing in  
1130 frontal cortex. *Nature*, 444(7117), 374–377. <https://doi.org/10.1038/nature05279>
- 1131 Stevenson, S. B., Volkmann, F. C., Kelly, J. P., & Riggs, L. A. (1986). Dependence of visual  
1132 suppression on the amplitudes of saccades and blinks. *Vision Research*, 26(11), 1815–  
1133 1824. [https://doi.org/10.1016/0042-6989\(86\)90133-1](https://doi.org/10.1016/0042-6989(86)90133-1)
- 1134 Thakkar, K. N., & Rolfs, M. (2019). Disrupted Corollary Discharge in Schizophrenia: Evidence  
1135 From the Oculomotor System. *Biological Psychiatry: Cognitive Neuroscience and*  
1136 *Neuroimaging*, 4(9), 773–781. <https://doi.org/10.1016/j.bpsc.2019.03.009>
- 1137 Thiele, A., Henning, P., Kubischik, M., & Hoffmann, K.-P. (2002). Neural mechanisms of  
1138 saccadic suppression. *Science (New York, N.Y.)*, 295(5564), 2460–2462.  
1139 <https://doi.org/10.1126/science.1068788>
- 1140 van Beers, R. J. (2007). The sources of variability in saccadic eye movements. *The Journal of*  
1141 *Neuroscience: The Official Journal of the Society for Neuroscience*, 27(33), 8757–8770.  
1142 <https://doi.org/10.1523/JNEUROSCI.2311-07.2007>
- 1143 van Opstal, A. J., & van Gisbergen, J. A. (1989). Scatter in the metrics of saccades and  
1144 properties of the collicular motor map. *Vision Research*, 29(9), 1183–1196.  
1145 [https://doi.org/10.1016/0042-6989\(89\)90064-3](https://doi.org/10.1016/0042-6989(89)90064-3)
- 1146 Vaziri, S., Diedrichsen, J., & Shadmehr, R. (2006). Why Does the Brain Predict Sensory  
1147 Consequences of Oculomotor Commands? Optimal Integration of the Predicted and the

- 1148        Actual Sensory Feedback. *Journal of Neuroscience*, 26(16), 4188–4197.
- 1149        <https://doi.org/10.1523/JNEUROSCI.4747-05.2006>
- 1150        von Helmholtz, H. (1924). *Helmholtz's treatise on physiological optics*, Vol. 1, *Trans. From the*  
1151        *3rd German ed* (pp. xxi, 482). Optical Society of America. <https://doi.org/10.1037/13536-000>
- 1153        Wald, A. (1945). Sequential Tests of Statistical Hypotheses. *The Annals of Mathematical*  
1154        *Statistics*, 16(2), 117–186. <https://doi.org/10.1214/aoms/1177731118>
- 1155        Wei, X.-X., & Stocker, A. A. (2015). A Bayesian observer model constrained by efficient coding  
1156        can explain “anti-Bayesian” percepts. *Nature Neuroscience*, 18(10), 1509–1517.  
1157        <https://doi.org/10.1038/nn.4105>
- 1158        Weiss, Y., Simoncelli, E. P., & Adelson, E. H. (2002). Motion illusions as optimal percepts.  
1159        *Nature Neuroscience*, 5(6), 598–604. <https://doi.org/10.1038/nn0602-858>
- 1160        Wurtz, R. H. (2018). Corollary Discharge Contributions to Perceptual Continuity Across  
1161        Saccades. *Annual Review of Vision Science*, 4, 215–237.  
1162        <https://doi.org/10.1146/annurev-vision-102016-061207>
- 1163        Wurtz, R. H., McAlonan, K., Cavanaugh, J., & Berman, R. A. (2011). Thalamic pathways for  
1164        active vision. *Trends in Cognitive Sciences*, 15(4), 177–184.  
1165        <https://doi.org/10.1016/j.tics.2011.02.004>
- 1166        Zimmermann, E., Morrone, M. C., Fink, G. R., & Burr, D. (2013). Spatiotopic neural  
1167        representations develop slowly across saccades. *Current Biology: CB*, 23(5), R193-194.
- 1168        Zuber, B. L., & Stark, L. (1966). Saccadic suppression: Elevation of visual threshold associated  
1169        with saccadic eye movements. *Experimental Neurology*, 16(1), 65–79.  
1170        [https://doi.org/10.1016/0014-4886\(66\)90087-2](https://doi.org/10.1016/0014-4886(66)90087-2)